

# Modelling photochemical pollutants in a deep urban street canyon: Application of a coupled two-box model approximation

Zhong, Jian; Cai, Xiaoming; Bloss, William

DOI:

[10.1016/j.atmosenv.2016.08.027](https://doi.org/10.1016/j.atmosenv.2016.08.027)

License:

Creative Commons: Attribution-NonCommercial-NoDerivs (CC BY-NC-ND)

*Document Version*

Peer reviewed version

*Citation for published version (Harvard):*

Zhong, J, Cai, X & Bloss, W 2016, 'Modelling photochemical pollutants in a deep urban street canyon: Application of a coupled two-box model approximation', *Atmospheric Environment*, vol. 143, pp. 86-107. <https://doi.org/10.1016/j.atmosenv.2016.08.027>

[Link to publication on Research at Birmingham portal](#)

## **Publisher Rights Statement:**

Checked for eligibility: 12/08/2016

## **General rights**

Unless a licence is specified above, all rights (including copyright and moral rights) in this document are retained by the authors and/or the copyright holders. The express permission of the copyright holder must be obtained for any use of this material other than for purposes permitted by law.

- Users may freely distribute the URL that is used to identify this publication.
- Users may download and/or print one copy of the publication from the University of Birmingham research portal for the purpose of private study or non-commercial research.
- User may use extracts from the document in line with the concept of 'fair dealing' under the Copyright, Designs and Patents Act 1988 (?)
- Users may not further distribute the material nor use it for the purposes of commercial gain.

Where a licence is displayed above, please note the terms and conditions of the licence govern your use of this document.

When citing, please reference the published version.

## **Take down policy**

While the University of Birmingham exercises care and attention in making items available there are rare occasions when an item has been uploaded in error or has been deemed to be commercially or otherwise sensitive.

If you believe that this is the case for this document, please contact [UBIRA@lists.bham.ac.uk](mailto:UBIRA@lists.bham.ac.uk) providing details and we will remove access to the work immediately and investigate.

# 1    **Modelling photochemical pollutants in a deep urban street canyon:** 2    **Application of a coupled two-box model approximation**

3    **Jian Zhong, Xiao-Ming Cai\* and William James Bloss**

4    School of Geography, Earth & Environmental Sciences, University of Birmingham, Edgbaston, Birmingham,  
5    B15 2TT, UK

6    *\*Corresponding author. Tel.: (0121) 4145533; Fax: (0121) 4145528.*

7    *Email address: x.cai@bham.ac.uk (X.-M. Cai).*

## 8    **Abstract:**

9    Air pollution associated with road transport is a major environmental issue in urban areas. Buildings  
10   in urban areas are the artificial obstacles to atmospheric flow and cause reduced ventilation for  
11   street canyons. For a deep street canyon, there is evidence of the formation of multiple segregated  
12   vortices, which generate flow regimes such that pollutants exhibit a significant contrast between  
13   these vortices. This results in poor air ventilation conditions at pedestrian level, thereby leading to  
14   elevated pollutant levels and potential breaches of air quality limits. The hypothesis of a well-mixed  
15   deep street canyon in the practical one-box model approach is shown to be inappropriate. This study  
16   implements a simplified simulation of the canyon volume: a coupled two-box model with a reduced  
17   chemical scheme to represent the key photochemical processes with timescales similar to and  
18   smaller than the turbulent mixing timescale. The two-box model captures the significant pollutant  
19   contrast between the lower and upper parts of a deep street canyon, particularly for NO<sub>2</sub>. Core  
20   important parameters (i.e. heterogeneity coefficient, exchange velocity and box height ratio) in the  
21   two-box model approach were investigated through sensitivity tests. The two-box model results  
22   identify the emission regimes and the meteorological conditions under which NO<sub>2</sub> in the lower  
23   canyon (i.e. the region of interest for the assessment of human health effects) is in breach of air  
24   quality standards. Higher NO<sub>2</sub> levels were observed for the cases with higher heterogeneity

coefficients (the two boxes are more segregated), with lower exchange velocities (worse ventilation conditions), or with smaller box height ratios (reduced dilution possibly due to secondary smaller eddies in the lower canyon). The performance of a one-box model using the same chemical scheme is also evaluated against the two-box model. The one-box model was found to systematically underestimate  $\text{NO}_2$  levels compared with those in the lower box of the two-box model for all the test scenarios. This underestimation generally tends to worsen for higher heterogeneity coefficients, lower exchange velocities or smaller box height ratios. This study highlights the limitation of the assumption of homogeneity in single box models for street canyon simulation, and the inherent uncertainties that must be borne in mind to appropriately interpret such model output (in particular, that a single-box treatment will systematically underestimate  $\text{NO}_2$  as experienced at street level).

**Keywords:** Air pollution; Urban street canyon; Two-box model; Dynamics; Photochemistry.

## 45    **1 Introduction**

46    Air pollution associated with road transport is a major environmental issue in urban areas (Murena  
47    et al., 2009). A street canyon is a typical urban configuration with surrounding buildings along the  
48    street (Li et al., 2008). Buildings in urban areas are the artificial obstacles to urban atmospheric  
49    flow (Salim et al., 2011) and cause reduced ventilation for street canyons thereby leading to air  
50    pollution levels potentially much greater than air quality objectives (Sahm et al., 2002). The most  
51    fundamental geometrical model of an urban street is a single infinitely long street with buildings of  
52    the same height on both sides, normally termed as the two-dimensional (2D) idealised street canyon  
53    with perpendicular flow (Liu et al., 2011). The characteristics of recirculation in a 2D idealised  
54    street canyon are strongly dependent upon the canyon aspect ratio ( $AR$ ), which is defined as the  
55    ratio of building height  $H$  to street width  $W$ . Under neutral meteorological conditions, the flow  
56    patterns can be classified into three regimes (Oke, 1987): isolated roughness ( $AR < 0.3$ ), wake  
57    interference ( $0.3 < AR < 0.7$ ) and skimming flow ( $AR > 0.7$ ). Skimming flow representing the worst-  
58    case scenario for pollutant dispersion normally occurs in regular street canyons ( $0.7 < AR < 1.5$ ) and  
59    deep street canyons ( $AR > 1.5$ ) (Murena et al., 2009). A single primary vortex is typically formed  
60    within regular street canyons (e.g.  $AR = 1$ ) (Baker et al., 2004). However, there is evidence of  
61    formation of multiple vortices within deep street canyons (e.g. Zhong et al. (2015); Li et al. (2009)),  
62    which can lead to greater contrasts in vertical pollutant distributions and create even poorer  
63    ventilation conditions for pollutants at the bottom of the canyon.

64    Many previous canyon modelling studies treated air pollutants as passive scalars (i.e. non-reactive  
65    pollutants) in street canyons as a first-order approximation. Caton et al. (2003) suggested three  
66    fundamental mechanisms that determine the concentration of a passive scalar in a 2D idealised  
67    street canyon, i.e. the emission rate, the advection-diffusion within the canyon, and the turbulent  
68    exchange (transfer) at the canyon roof level. For a practical application, the turbulent exchange  
69    mechanism is a major research challenge as this plays the key role in controlling the pollutant  
70    abundance in the street canyon (Barlow et al., 2004). This phenomenon can be represented by a

71 simplified parameter called ‘transfer velocity’ (Salizzoni et al., 2009) or ‘air ventilation rate’ (Liu  
72 and Leung, 2008), herein referred to as ‘exchange velocity’ (Bright et al., 2013), which is  
73 responsible for quantifying the exchange of mass between the street canyon and the overlying  
74 atmospheric boundary layer. However, many emissions from vehicles are reactive, evolving  
75 chemically as the air parcel is circulated inside the street canyon and exchanged with the air above  
76 the rooftop. Consequently, chemical processes, alongside dispersion and transport, are expected to  
77 play an important role in determining the abundance of reactive pollutants. Zhong et al. (2014)  
78 employed photochemical box models to investigate the segregation effects of heterogeneous  
79 emissions on ozone ( $O_3$ ) levels in idealised urban street canyons and evaluate their uncertainty  
80 when grid-averaged emissions were adopted. Their study provides a simple and easy approach to  
81 consider the effects of both chemistry and dynamics using box models with a wide range of  
82 emission scenarios, but was restricted to idealised street canyons (completely segregated) with  
83 emission heterogeneity between them. Liu and Leung (2008) developed a one-box (chemistry)  
84 model to study reactive pollutant dispersion in street canyons ( $AR=0.5, 1, 2$ ), using exchange  
85 velocity values derived from large-eddy simulations (LES) for different canyon ARs (Liu et al.,  
86 2005). Such models are unable to reproduce the significant contrasts of pollutant concentration  
87 between the lower and upper canyon regions, exacerbated in deep street canyons, since the whole  
88 canyon is treated as one well-mixed box for all ARs. Li et al. (2009) found that pollutants were at  
89 extremely high levels near the street level in deep street canyons. Field measurements in deep street  
90 canyons (Murena and Favale (2007); Murena et al. (2008)) also indicated that pollutant  
91 concentrations at pedestrian level in deep street canyons could be up to three times that in regular  
92 street canyons. Murena et al. (2011) and Murena (2012) attempted to implement a simplified two-  
93 box model (for passive scalars) with regard to the prediction of carbon monoxide (CO)  
94 concentrations in deep street canyons. The mass transfer between the two adjacent boxes inside the  
95 canyon is expressed by introducing an ‘exchange velocity’. Their study provided a useful guidance  
96 for improving the performance of the street-canyon operational models, e.g. Operational Street

97 Pollution Model (OSPM) (Buckland, 1998), which might otherwise be unreliable while applied into  
98 a deep street canyon since they were developed for street canyons with unity aspect ratio. CO in  
99 their two-box model was effectively considered a passive scalar (a reasonable approximation as CO  
100 has a long chemical lifetime (weeks) in the troposphere) and therefore no chemical processing was  
101 taken into account. Zhong et al. (2015) adopted a two-box model with the incorporation of simple  
102  $\text{NO}_x\text{-O}_3$  photochemistry, based on the existence of two vortices in a deep street canyon as  
103 characterised typical LES simulations. Their study enabled the consideration of reactive pollutants  
104 for the two-box model approach. However, only simple chemistry was considered, without the  
105 consideration of the volatile organic compounds (VOCs) processing (which may result in the  
106 additional conversion of nitric oxide (NO) to nitrogen dioxide ( $\text{NO}_2$ )) and production of  $\text{O}_3$ . Zhong  
107 et al. (2016) presented a comprehensive review of the recent numerical modelling studies that  
108 couple the dynamics and chemistry of reactive pollutants in urban street canyons. The  
109 computational fluid dynamics (CFD) modelling approach can provide high spatial and temporal  
110 resolution simulations of flow and pollutant fields within street canyons (e.g. Zhong et al. (2015);  
111 Bright et al. (2013); Kwak et al. (2013); Li et al. (2012)). However, they normally require a high  
112 level of computational resource and substantial input information (e.g. computational domain, flow  
113 characteristics, boundary conditions, and chemical schemes). As an alternative tool, the box model  
114 approach is relatively simple to use and permits relatively complex chemistry to be afforded in  
115 street canyon modelling such that it might provide a simpler tool to explore to air pollution issues  
116 for policy makers. Such box models normally require far less computational cost than CFD models.  
117 However, due to the inherent semi-empirical assumptions, box models are unable to reproduce the  
118 detailed distribution of the flow or pollutant fields in street canyons.

119 The two-box models of Murena et al. (2011) and Murena (2012) for an effective passive scalar or  
120 Zhong et al. (2015) with the simple  $\text{NO}_x\text{-O}_3$  photochemistry have successfully captured the contrast  
121 between the bulk concentration in the lower street box and that in the upper street box. The present  
122 study will extend the coupled two-box model approach so that it considers both  $\text{NO}_x$  and VOCs

chemical processing under a variety of wind conditions for a wide range of emission scenarios, as a computationally efficient complement to (e.g.) full CFD simulations. The performance of a one-box model with the same chemical scheme will be evaluated compared with the more comprehensive two-box model. The methodology concerning the implementation of the two-box model with the complex chemistry is described in Section 2. Various factors affecting the performance of the two-box model are investigated and discussed in Section 3 and conclusions are presented in Section 4.

## 2 Framework of a coupled two-box model approximation

### 2.1 Model setup

In the box model approach, a well-mixed hypothesis is adopted, i.e. the air inside the box is assumed to be well-mixed. The box model is a simple approach to describe the evolution of air pollutants, which only requires low computational cost. For deep street canyons, the presence of two primary counter-rotating vortices segregates the street-canyon flow into layers with contrasting dynamical features so that pollutants exhibit a significant reduction with building height; this has been reported in the literature (Murena and Favale, 2007). In such situations, the “well-mixed” assumption tends to fail (Murena et al., 2011). Therefore, a more realistic model treatment (i.e. a two-box model) is needed to capture the vertically segregated layers with a significant concentration contrast and the communication between vortices in the deep street canyon. The deep street canyon can be divided into two boxes (conceptualised in Figure 1a) with the corresponding vortex inside each box separated by using a plane at the level of  $z/H = \alpha$  (where  $\alpha$  is the box height ratio determined by the flow structure with the street canyon). It is assumed that each vortex has sufficient intensity for the chemical species to be well-mixed within the corresponding box (Murena et al., 2011). The mathematical description of the two-box model is as follows:

$$\frac{dC_{i,L}}{dt} = -\frac{w_{t,L}}{H_L} (C_{i,L} - C_{i,U}) + E_{i,L} + \Delta S_{i,L} \quad (1)$$

$$\frac{dC_{i,U}}{dt} = \frac{w_{t,L}}{H_U} (C_{i,L} - C_{i,U}) - \frac{w_{t,U}}{H_U} (C_{i,U} - C_{i,b}) + \Delta S_{i,U} \quad (2)$$

where  $C_{i,L}$  (ppb) and  $C_{i,U}$  (ppb) are the concentrations of the  $i^{th}$  species in the lower and upper boxes, respectively;  $t$  (s) is the time;  $H_L$  (m) and  $H_U$  (m) are the heights of the lower and upper boxes, respectively;  $w_{t,L}$  ( $\text{m s}^{-1}$ ) is the exchange velocity between the lower and upper boxes, and  $w_{t,U}$  ( $\text{m s}^{-1}$ ) is the exchange velocity between the upper box and the overlying background atmosphere;  $E_{i,L}$  ( $\text{ppb s}^{-1}$ ) is the emission rates of the  $i^{th}$  species released from the lower canyon;  $\Delta S_{i,L}$  ( $\text{ppb s}^{-1}$ ) and  $\Delta S_{i,U}$  ( $\text{ppb s}^{-1}$ ) are the chemical source terms of the  $i^{th}$  species in the lower and upper boxes, respectively. A reduced chemical scheme (RCS), developed and validated by Bright et al. (2013), is adopted as the chemical mechanism in this study for the derivation of the chemical source terms to be used in Equations 1-2. The RCS includes 51 chemical species and 136 chemical reactions (Table A1 in the Appendix A). The two-box model approach without the consideration of chemistry (i.e. the chemical source terms in Equations 1-2 are zero and an effective passive (non-reactive) scalar is assumed) was initially developed and evaluated by Murena et al. (2011) and Murena (2012) based on the information from steady-state CFD simulations of deep street canyons. Subsequently, the two-box model approach considering simple  $\text{NO}_x\text{-O}_3$  photochemistry (i.e. the chemical source terms in Equations 1-2 are derived from simple  $\text{NO}_x\text{-O}_3$  photochemistry) was implemented by Zhong et al. (2015) based on the LES simulations of two vortices formed within a deep street canyon. These previous studies provide confidence that the simulated dynamics (exchange velocities) adopted for the street canyon boxes is reasonable although ideally such box models would be tested against observations (but these are as yet very scarce). This study attempts to extend the application of two-box model approach by considering relatively more complex chemistry (i.e. the RCS chemical mechanism).

The one-box model (with the “well-mixed” assumption for the whole deep street canyon) is conceptualised in Figure 1b and formulated below:



$$\frac{d}{dt}C_{i,0}(t) = E_{i,0} - \frac{w_{t,0}}{H_0}(C_{i,0} - C_{i,b}) + \Delta S_{i,0} \quad (3)$$

where the symbols are similar to those in the two-box model (the quantities associated are denoted as “0” rather than the “U” and “L” in the two-box model approach).

We assume that  $C_{i,L}$  from the more sophisticated and realistic two-box model is the “true” value (in the sense that  $C_{i,L}$  is closer to the true value in comparison with  $C_{i,0}$  from the one-box model). Thus, there will be an error for the “one-box” model due to the well-mixed assumption, compared with the concentration in the lower box (i.e. the interest area of potential exposure assessment for pedestrians) by the “two-box” model. This error can be expressed as the concentration difference due to segregation as follows:

$$\Delta C_{i,L} = C_{i,0} - C_{i,L} \quad (4)$$

Then we can define the percentage of overestimation by the “one-box” model compared with the concentration in the lower box by the “two-box” model:

$$\phi_{i,L}(t) = \frac{\Delta C_{i,L}(t)}{C_{i,L}(t)} \times 100\% \quad (5)$$

If  $\phi_{i,L}(t) = 0\%$ , it means that the “one-box” model is in agreement with the “two-box” model; If  $\phi_{i,L}(t) > 0\%$  or  $\phi_{i,L}(t) < 0\%$ , it means that the “one-box” model over- or under-estimates the concentration compared with the “two-box” model.

## 2.2 Exchange velocities in the two-box model

Exchange velocities implemented into the two-box model can be determined from a comprehensive numerical flow model (e.g. the Reynolds-Averaged Navier-Stokes model or large-eddy simulation) by calculating the ventilation of a passive scalar once the boundaries of the two boxes are defined. According to Fick’s law, the flux of a passive scalar (denoted as “ps”),  $F_{ps}$  (ppb m s<sup>-1</sup>), between

191 the lower and upper boxes under the steady state (the “two-box” model approach) can be written as  
 192 follows,

$$193 \quad F_{ps} = w_{t,L}(C_{ps,L} - C_{ps,U}) \quad (6)$$

194 Similarly, the flux between the upper box and the background air under the steady state must be  
 195 equal to the flux in (6) and it can be expressed as:

$$196 \quad F_{ps} = w_{t,U}(C_{ps,U} - C_{ps,b}) \quad (7)$$

197 If the whole street canyon is considered as one box, the flux of a passive scalar for the whole box  
 198 under the steady state (one-box model approach) is derived as:

$$199 \quad F_{ps} = w_{t,0}(C_{ps,0} - C_{ps,b}) \quad (8)$$

200 We should also have the following equation due to the definitions of the three concentrations and  
 201 the volumes of the boxes:

$$202 \quad C_{ps,0} = \alpha C_{ps,L} + (1 - \alpha)C_{ps,U} \quad (9)$$

203 Equation 9 can be rewritten as:

$$204 \quad C_{ps,0} = C_{ps,U} + \alpha(C_{ps,L} - C_{ps,U}) \quad (10)$$

205 Here,  $\alpha \in (0,1)$  is the ratio of the lower box’s volume to the volume of the whole canyon. When an  
 206 idealised street canyon is considered,  $\alpha$  becomes the box height ratio,  $H_L/H_0$ .  $H_L$  can be determined  
 207 by the flow structure within the street canyon, namely, the height of the lower vortex.

208 In this study, it is assumed that  $C_{ps,b} = 0$ , i.e. ‘zero background’ is assumed for a passive scalar (e.g.  
 209 Murena et al. (2011) ; Murena (2012); Zhong et al. (2015)). According to Equations 7 and 8, it can  
 210 be derived that  $\frac{w_{t,0}}{w_{t,U}} = \frac{C_{ps,U}}{C_{ps,0}}$ , which denotes the ratio of the upper canyon concentration ( $C_{ps,U}$ ) to

211 the whole canyon averaged concentration ( $C_{ps,0}$ ) and represents the deviation from the homogenous  
 212 system (assuming the whole canyon as a well-mixed box). It is also assumed that  $C_{ps,L} \geq C_{ps,U}$  is  
 213 the case for passive scalars emitted from street canyons near the ground level (Figure 2). According  
 214 to Equation 10,  $C_{ps,0} \geq C_{ps,U}$  and  $w_{t,0} \leq w_{t,U}$  can be derived. Then we may also define a non-  
 215 dimensional parameter to represent the heterogeneity coefficient (or spatial variation) across the two  
 216 boxes, i.e.

$$217 \quad \eta = 1 - \frac{w_{t,0}}{w_{t,U}} \quad (11)$$

218 where  $\eta \in [0,1]$ . If  $\eta = 0$ , then  $w_{t,0} = w_{t,U}$  from Equation **Error! Reference source not found.** and  
 219 it yields  $C_{ps,0} = C_{ps,U}$  according to Equations 7 and 8, and  $C_{ps,U} = C_{ps,L}$  based on Equation 10.  
 220 Thus, the two boxes are homogenous. Higher (or lower) values of  $\eta$  represent the two boxes that  
 221 are more (or less) segregated; in other words, the simulation possesses more (or less) heterogeneity.  
 222 According to Equations 6-9, it can be derived that:

$$223 \quad \frac{1}{w_{t,0}} = \frac{\alpha}{w_{t,L}} + \frac{1}{w_{t,U}} \quad (12)$$

224 Based on Equations 6-12, exchange velocities for the two-box model are obtained as follows:

$$225 \quad w_{t,U} = \frac{w_{t,0}}{(1-\eta)} \quad (13)$$

$$226 \quad w_{t,L} = \frac{\alpha w_{t,0}}{\eta} \quad (14)$$

227 The physical mechanisms that determine the value of the heterogeneity coefficient ( $\eta$ ) are explained  
 228 below. For a given  $\alpha$  (i.e. fixed sizes of the two vortices), the heterogeneity coefficient may be  
 229 determined by the spatial pattern of turbulence, which could in turn be affected by the building

geometry, local wind conditions, local turbulence generated by moving vehicles or thermal forcing,  
 and damped turbulence by (e.g.) tree leaf or stable atmosphere factors. For example, greater local  
 vehicle generated turbulence (or other factors) transfers more pollutants from the lower box into the  
 upper box, giving a lower value of  $C_{ps,L}$  and a higher value of  $C_{ps,U}$ . Based on Equation 7, a lower  
 value of  $w_{t,U}$  is yielded. Then a lower value of  $\eta$  is obtained based on Equation **Error! Reference**  
**source not found.**; namely, the two-box system possesses less heterogeneity. If only the wind  
 speed above the canyon is considered and the exchange velocity is assumed to be scaled with the  
 wind speed (Murena et al. (2011) and Murena (2012)) for a given building geometry,  $\eta$  would  
 remain unchanged (i.e. the ratio of exchange velocities in Equation 11 remains unchanged). Value  
 of  $\eta$  may vary with the AR of the canyon, i.e. a larger AR (deeper canyon) may give a higher value  
 of  $\eta$  due to the worse ventilation conditions. Also, lower turbulence caused by a stable atmosphere  
 (Ramamurthy et al., 2007) and decoupling caused by an elevated tree-leaf canopy (Gromke and  
 Ruck, 2012) may give higher values of  $\eta$ .

## 2.3 Model Scenarios

Table 1 gives an overview of the case settings. For the BASE case, these parameters are set as:  
 $\eta = 0.5$ ,  $w_{t,0} = 0.02 \text{ m s}^{-1}$  and  $\alpha = 0.5$ , which represent a typical urban scenario. The value of  
 $\eta = 0.5$  represents a median level of heterogeneity, i.e. the pollutant concentration in the lower (or  
 upper) box is 50% higher (or lower) than the mean concentration averaged over the whole canyon  
 for a given  $\mathcal{A}$  of 0.5. In other words, the concentration in the lower box is 3 times that in the upper  
 box, which could be the case for deep street canyons (Murena and Favale (2007); Murena et al.  
 (2008)). The value for  $w_{t,0} = 0.02 \text{ m s}^{-1}$  is used based on those derived from large-eddy simulations  
 for street canyons (e.g. Zhong et al. (2015); Bright et al. (2013)) while the reference incoming wind  
 speed is about  $2 \text{ m s}^{-1}$ . This investigation is focused on highly polluted scenarios, i.e. calm wind  
 blowing across the street canyon rather than windy conditions.  $w_{t,0}$  is assumed to scale with the  
 reference wind speed above the street canyon (Murena et al. (2011) and Murena (2012)) while

255 keeping the same turbulence pattern. The value of  $\alpha = 0.5$  represents equal size vortices (volume of  
 256 air) for both lower and upper boxes (e.g. found in the CFD study by Kwak et al. (2013)), which  
 257 represents a typical situation for deep street canyons. To investigate the effect of  $\eta$ , the values of  
 258 other parameters are assumed to kept the same as those used in Case BASE and a series of values of  
 259  $\eta$  are considered, i.e. Case HC-LL ( $h = 0.1$ ), Case HC-L ( $\eta = 0.3$ ), Case HC-H ( $\eta = 0.7$ ) and Case  
 260 HC-HH ( $\eta = 0.9$ ). Likewise, a series of other cases together with their parameters are also  
 261 summarised in Table 1, i.e. the effect of varying  $w_{t,0}$  with Case EX-LL ( $w_{t,0} = 0.012 \text{ m s}^{-1}$ ), Case  
 262 EX-L ( $w_{t,0} = 0.016 \text{ m s}^{-1}$ ), Case EX-H ( $w_{t,0} = 0.024 \text{ m s}^{-1}$ ) and Case EX-HH ( $w_{t,0} = 0.028 \text{ m s}^{-1}$ );  
 263 and the effect of varying  $a$  with Case HB-LL ( $a = 0.1$ ), Case HB-L ( $a = 0.3$ ), Case HB-H ( $a = 0.7$ ),  
 264 and Case HB-HH ( $a = 0.9$ ). As both  $\eta$  and  $\alpha$  range from 0 to 1, our tests of (0.1, 0.9) for both  
 265 parameters covers a wide range of most possible scenarios. Our tests of (0.012, 0.028)  $\text{m s}^{-1}$  for the  
 266 exchange velocity are mainly focus on the sensitivity to this typical situation (0.02  $\text{m s}^{-1}$  for Case  
 267 BASE). For each case, the corresponding ‘one-box’ model and the ‘two-box’ model were run  
 268 (Figure 1). Figure 3 illustrated the exchange velocities (based on Equations 13-14) implemented in  
 269 the ‘two-box’ model for the scenarios in Table 1, considering the effect of  $\eta$ ,  $w_{t,0}$  and  $a$ ,  
 270 respectively. Figure 3a shows that, for a given  $\alpha = 0.5$  and  $w_{t,0} = 0.02 \text{ m s}^{-1}$ , as  $\eta$  increases,  $w_{t,L}$   
 271 increases, but  $w_{t,U}$  decreases. Figure 3b shows that, for a given  $\alpha = 0.5$  and  $\eta = 0.5$ , as  $w_{t,0}$   
 272 increases, both  $w_{t,L}$  and  $w_{t,U}$  increases linearly. This linear relationship is also found in the  
 273 literature (Murena et al., 2011). Figure 3c shows that, for a given  $\eta = 0.5$  and  $w_{t,0} = 0.02 \text{ (m s}^{-1}\text{)}$ , as  
 274  $\alpha$  increases,  $w_{t,L}$  remains the same level, but  $w_{t,U}$  increases linearly.

275 For each case (listed in Table 1), the corresponding ‘one-box’ model and the ‘two-box’ model were  
 276 run (Figure 1). Initial and background conditions of chemistry used in this study follow those of  
 277 Zhong et al. (2014), in which the independent photochemical box model is initially spun up to allow  
 278 concentrations of all 51 species in RCS to be calculated. In order to characterise a wide range of

279 real scenarios, the representative  $E_{NOx}$  and  $E_{VOCs}$  are scaled by different factors of between 0.1 and 2  
280 applied to those of the “Typical Real-world Emission Scenario” (TRES) (i.e. 620, 128 and 1356 g  
281  $km^{-1} hr^{-1}$  for emission rates for  $NO_x$ , VOCs and CO, respectively) (Zhong et al., 2014), which  
282 represents an urban continuous road traffic of 1500 vehicles  $h^{-1}$  with an average speed of 30 mph  
283 and a vehicle fleet composition for the UK in the year 2010.

284 The lower street canyon is the volume of interest for the assessment of human health effects (i.e.  
285 where exposure occurs).  $NO_2$  is an important photochemical pollutant and the issue of  $NO_2$  air  
286 pollution has become an urgent agenda for the urban air quality management (Defra, 2015). This  
287 article will focus on the effects of  $\eta$  (heterogeneity coefficient) and  $w_{t,0}$  (exchange velocity), and  
288  $\alpha$  (box height ratio) on the  $NO_2$  characteristics in the lower canyon (box), once photochemical box  
289 models have reached a quasi-steady state. The coupled two-box model represents the key  
290 photochemical processes with timescales similar to and smaller than the turbulent mixing timescale  
291 in street canyons. The typical time scale for the street canyon air to exchange with the external flow  
292 aloft is  $H_0 / w_{t,0}$ , which is an order of 10 min (Bright et al. (2013)). Although the chemistry system  
293 is complex and highly nonlinear, possessing a wide range of chemical time scales, the box model  
294 will eventually achieve a quasi-steady state (pollutants remain nearly constants) as the run time is  
295 much larger than the exchange timescale, leaving those slow chemical reactions still slightly  
296 ‘unsteady’ (Bright et al. (2013)).

## 297 **3 Results and discussion**

### 298 **3.1 Effect of the heterogeneity coefficient**

299 Figure 4 illustrates the effect of the heterogeneity coefficient ( $\eta$ ) on  $C_{NO_2,L}$  (ppb), i.e. the  $NO_2$   
300 concentration in the lower box, for (a) Case HC-LL ( $\eta=0.1$ ), (b) Case HC-L ( $\eta=0.3$ ), (c) Case  
301 BASE ( $\eta=0.5$ ), (d) Case HC-H ( $\eta=0.7$ ), (e) Case HC-HH ( $\eta=0.9$ ) and (f) Selected lines for  
302 analysis. In Figure 4,  $E_{VOCs}$  and  $E_{NOx}$  are normalised to the corresponding values in the “Typical

Real-world Emission Scenario” (TRES, represented by  $\triangle$ ), derived from the fleet composition for the year 2010. The trajectory 2005-2020 shown in Figure 4 (line on each panel) represents the changing emission scenarios for 2005 to 2020, derived from the UK fleet composition projections (NAEI, 2003) and the UK Road Vehicle Emission Factors (Boulter et al., 2009) assuming constant traffic volumes and speeds equal to those in the ‘TRES’ scenario for 2010 - i.e. only the emission change with vehicle technology and fleet composition is considered, rather than traffic growth. The solid red curves highlight the UK air quality standard for hourly  $\text{NO}_2$  (105 ppb) (no exceedances more than 18 times a year) (Defra, 2008). It is interesting to note that  $C_{\text{NO}_2,L}$  generally has a similar pattern for the cases and increases with the heterogeneity coefficient from 0.1 (Figure 4a) to 0.9 (Figure 4e). This can be explained by the reducing exchange between the lower and upper box (indicated by a lower value of  $w_{t,L}$  when  $\eta$  is large in Figure 3a). The higher heterogeneity coefficient may also be considered to reflect less local traffic produced turbulence in the lower box, as this would reduce the air ventilation from the lower box to the upper box. This is consistent with the finding by Murena et al. (2011) that there would be a lower exchange velocity between the lower and upper box and a higher level of pollutant concentration in the lower box for the case without considering the local traffic produced turbulence. This indicates that heterogeneity in the street canyon significantly affects pollutant concentrations in the lower box. Therefore, it is not surprising that the solid red curve shifts from the higher emission region to the lower emission region as the heterogeneity coefficient increases (Figure 4a-e). The curve shift (or more generally, the pattern shift) is not linear, mainly due to the highly non-linear chemical regimes. It is also noted that emissions at the TRES level are expected to lead to  $\text{NO}_2$  concentrations in breach of the UK air quality standard for hourly  $\text{NO}_2$ , for this idealised scenario, while the heterogeneity coefficient is larger than 0.5 (Figure 4c-e). It is observed that trajectory 2005-2020 cuts across the solid red curve. This indicates the importance of future technology in the expected reduction of  $\text{NO}_2$  levels thereby meeting the UK  $\text{NO}_2$  air quality standards over years (although we note that such anticipated reduction may not be fully realised (Carslaw and Rhys-Tyler, 2013)). For a heterogeneity

329 coefficient of 0.9, the UK air quality standard for hourly  $\text{NO}_2$  is breached for most years, for this  
330 idealised scenario. This indicates that it is important to improve the air ventilation within the street  
331 canyon, thereby decreasing the heterogeneity coefficient leading to better air quality and reduced  
332 pedestrian exposure.

333 Figure 5 shows the transects of  $C_{\text{NO}_2,L}$  (ppb) for Case HC-LL, Case HC-L, Case BASE, Case HC-H  
334 and Case HC-HH through the selected lines for analysis in Figure 4f. The dashed line in Figure 4f  
335 (“Fixed  $E_{\text{NO}_x}$ ”) represents a technology change targeting only  $E_{\text{VOCs}}$  from vehicles, or roads with a  
336 varying coverage of vegetation which may emit further VOCs into the urban canopy (Loughner et  
337 al., 2012). The dotted line in Figure 4f (“Fixed  $E_{\text{VOCs}}$ ”) represents a technology change targeting  
338 only  $E_{\text{NO}_x}$  from vehicles. The dot-dash line in Figure 4f (“TRES-2010”) represents a technology of  
339 both  $E_{\text{VOCs}}$  and  $E_{\text{NO}_x}$  with the proportional change in traffic emissions of both VOCs and  $\text{NO}_x$  from  
340 vehicles specified for the TRES. This dot-dashed line may also represent control of the number of  
341 vehicles in streets or scenarios for different areas (busier or less busy roads) with the same fleet  
342 composition as the TRES. The trajectory line (“Trajectory 2005-2020”) indicates emission  
343 scenarios for the years 2005 to 2020 with the same traffic volume and speed as the TRES. The  
344 corresponding results along the selected lines are analysed below.

345 Figure 5a shows that  $C_{\text{NO}_2,L}$  gradually increases with the increase of  $E_{\text{VOCs}}$  at a fixed  $E_{\text{NO}_x}$  (same as  
346 that of TRES). This can be explained as VOC-derived peroxy radicals can play a key role in the  
347 conversion of NO to  $\text{NO}_2$  through chemistry; in other words, for the fixed  $E_{\text{NO}_x}$ , the increase of  
348  $C_{\text{NO}_2,L}$  is mainly due to the chemical processing through VOCs. This indicates that all other factors  
349 being equal, slightly higher levels of  $\text{NO}_2$  will slightly result from more green (i.e. vegetated) areas  
350 producing extra  $E_{\text{VOCs}}$ . However, this neglects the depositional loss of  $\text{NO}_2$  to vegetation (Pugh et  
351 al., 2012). It is noted that the concentration difference of  $C_{\text{NO}_2,L}$  between Case HC-HH ( $\eta=0.9$ ) and  
352 Case HC-LL ( $\eta=0.1$ ) gradually increases with the increase of  $E_{\text{VOCs}}$ , from 23 ppb (at  
353  $E_{\text{VOCs}} / E_{\text{TRES,VOCs}}=0.1$ ) to 80 ppb (at  $E_{\text{VOCs}} / E_{\text{TRES,VOCs}}=2$ ). This finding indicates that the effect of



354 the heterogeneity coefficient is more significant for higher  $E_{VOCs}$  when keeping  $E_{NOx}$  unchanged.  
 355 Figure 5b shows that  $C_{NO_2,L}$  generally increases with the increase of  $E_{NOx}$  at a fixed  $E_{VOCs}$  (same as  
 356 that of TRES), with a rapid increase while  $E_{NOx} / E_{TRES,NOx}$  ranges from 0.1 to 0.5. This is mainly  
 357 attributed to the fact that the emitted  $NO_x$  contributes directly to the increase of  $C_{NO_2,L}$ . This  
 358 indicates that adoption of technology controlling  $NO_x$  will have a significant effect in reducing  $NO_2$   
 359 levels (as would be anticipated). The direct contributions of  $NO_x$  emissions to  $C_{NO_2,L}$  (assuming no  
 360 photochemical processes) for cases with different heterogeneity coefficients are indicated by a  
 361 series of radiating lines in Figure 5b. Any deviation from these radiating lines can be attributed to  
 362 the contributions from photochemical processes (which convert  $NO$  to  $NO_2$ ). It can be seen from  
 363 Figure 5b that the chemically induced  $NO_2$  increases rapidly for smaller  $E_{NOx}$  and becomes steady  
 364 for larger  $E_{NOx}$ . It is found that the contributions from photochemistry / ozone titration are dominant  
 365 over those from direct emissions, highlighting the importance of photochemistry in converting  $NO$   
 366 to  $NO_2$  for the street canyon environment. There is also clear evidence of the reduced impact of the  
 367 heterogeneity coefficient at lower  $E_{NOx}$ . The concentration difference of  $C_{NO_2,L}$  between Case HC-  
 368 HH and Case HC-LL gradually increases with the increase of  $E_{NOx}$ , from 13 ppb (at  $E_{NOx} / E_{TRES,NOx}$   
 369  $=0.1$ ) to 60 ppb (at  $E_{NOx} / E_{TRES,NOx} =2$ ). Figure 5c illustrates the change of  $C_{NO_2,L}$  for TRES-2010  
 370 with changing traffic volume only (i.e.  $E_{VOCs}$  and  $E_{NOx}$  varies proportionally). The pattern of  $C_{NO_2,L}$   
 371 is a combination of those in Figure 5a and Figure 5b, and a nearly linear relationship is observed.  
 372 This indicates that controlling the number of vehicles in street canyons with the same fleet  
 373 composition as the TRES will have an approximately linear effect on the  $NO_2$  levels. This evidence  
 374 may be used to derive a simple parameterisation scheme for  $NO_2$  with respect to traffic volume.  
 375 Figure 5d shows the results of  $C_{NO_2,L}$  from the year 2005 to 2020. It is observed that  $C_{NO_2,L}$   
 376 decreases with year. This is mainly attributed to the predicted performance of control technologies  
 377 applied, which achieve lower  $E_{VOCs}$  and  $E_{NOx}$ .  $C_{NO_2,L}$  begins to attain the air quality standard for  
 378 hourly  $NO_2$  (for this idealised scenario) from the year 2007 for Case HC-LL ( $\eta=0.1$ ), 2009 for

379 Case HC-L ( $\eta=0.3$ ), 2011 for Case BASE ( $\eta=0.5$ ), 2014 for Case HC-H ( $\eta=0.7$ ) and 2017 for  
380 Case HC-HH ( $\eta=0.9$ ).  $C_{NO_2,L}$  represents the mean concentration of the entire lower box which may  
381 still be substantially lower than the highest concentration in the hotspots near the exhaust zone  
382 (Zhong et al., 2015).

383 Figure 6 shows the effect of the heterogeneity coefficient ( $\eta$ ) on  $\phi_{NO_2,L}$  (%), i.e. the percentage of  
384 overestimation for NO<sub>2</sub> in the lower canyon, by the ‘one-box’ model, compared with the more  
385 sophisticated coupled-two-box model approach. Negative values of  $\phi_{NO_2,L}$  are observed for all the  
386 cases. It is interesting to notice that the magnitude of  $\phi_{NO_2,L}$  gradually increases with the increase of  
387 heterogeneity coefficient ( $\eta$ ), i.e. the range of (-9.54 %, -4.13 %) among all tested emission  
388 scenarios for Case HC-LL with  $\eta=0.1$  (Figure 6a), (-23.94 %, -11.36 %) for Case HC-L with  
389  $\eta=0.3$  (Figure 6b), (-33.49 %, -17.07 %) for Case BASE with  $\eta=0.5$  (Figure 6c), (-40.74 %, -  
390 21.94 %) for Case HC-H with  $\eta=0.7$  (Figure 6d) and (-46.73 %, -26.22 %) for Case HC-HH with  
391  $\eta=0.9$  (Figure 6e). It is also noted that  $\phi_{NO_2,L}$  changes nonlinearly with the change of emissions of  
392 NO<sub>x</sub> and VOCs, which is mainly attributed to nonlinear photochemical reactions. This indicates that  
393 for higher VOCs emission rate scenarios (Figure 6), nonlinear photochemistry plays a key role in  
394 reducing the percentage of overestimation for NO<sub>2</sub> by the ‘one-box’ model compared with that for  
395 e.g. a passive scalar.

396 Figure 7 illustrates the transects of  $\phi_{NO_2,L}$  (ppb) for Case HC-LL, Case HC-L, Case BASE, Case  
397 HC-H and Case HC-HH through the selected lines for analysis in Figure 4f. Figure 7a shows that  
398 the magnitude of  $\phi_{NO_2,L}$  slightly increases with the increase of  $E_{VOCs}$ , i.e. from -4.48 % to -4.59 %  
399 for  $\eta=0.1$ , from -11.88 % to -14.26 % for  $\eta=0.3$ , from -18.14% to -24.16 % for  $\eta=0.5$ , from -  
400 23.57 % to -33.54 % for  $\eta=0.7$  and from -28.37 % to -41.88 % for  $\eta=0.9$ . It is noted that the  
401 higher the value of heterogeneity coefficient, the larger the magnitude of  $\phi_{NO_2,L}$ . This indicates that  
402 the one box model performance is better for the case with lower heterogeneity coefficients or for

403 lower VOC emissions (or less “green”) areas. Figure 7b shows that the magnitude of  $\phi_{NO_2,L}$   
 404 generally decreases with the increase of  $E_{NO_x}$ , except for a slight increase at  $E_{NO_x} / E_{TRES,NO_x} = 0.2$  for  
 405 the cases with  $\eta = 0.5$ ,  $\eta = 0.7$  and  $\eta = 0.9$ . This may be attributed to the complexity of the nonlinear  
 406 photochemistry in such segregated street canyon environment. Figure 7c also shows that there is no  
 407 significant change in the  $\phi_{NO_2,L}$  when changing both  $E_{VOCs}$  and  $E_{NO_x}$  and that the values of  $\phi_{NO_2,L}$  are  
 408 principally affected by the heterogeneity coefficient ( $\eta$ ). This finding is also indicated by Figure 7d,  
 409 in which the values of  $\phi_{NO_2,L}$  do not change significantly over the simulated emissions evolution for  
 410 the years 2005 to 2020 (the maximum difference is within 5 %) and there is significant contrast  
 411 between the cases with a difference in heterogeneity coefficient (the contrast is around 10 % for the  
 412 interval of  $\eta = 0.2$ ).

### 413 **3.2 Effect of the exchange velocity**

414 Figure 8 illustrates the effect of the exchange velocity ( $w_{t,0}$ ) on  $C_{NO_2,L}$  (ppb), i.e. the concentration  
 415 in the lower box, for (a) Case EX-LL ( $w_{t,0} = 0.012 \text{ m s}^{-1}$ ), (b) Case EX-L ( $w_{t,0} = 0.016 \text{ m s}^{-1}$ ), (c)  
 416 Case BASE ( $w_{t,0} = 0.02 \text{ m s}^{-1}$ ), (d) Case EX-H ( $w_{t,0} = 0.024 \text{ m s}^{-1}$ ) and (e) Case EX-HH ( $w_{t,0}$   
 417  $= 0.028 \text{ m s}^{-1}$ ).  $w_{t,0}$  has a direct effect on the pollutant concentration in the one-box homogenous  
 418 system (also representing the whole canyon averaged pollutant concentration in the two-box system)  
 419 and plays an important role in determining the lower canyon pollutant concentration in the two box  
 420 system for given scenario conditions (Section 2).  $w_{t,0}$  can vary with the external wind turbulence  
 421 above the street canyon, the street canyon geometry and the stability of the atmosphere. It is  
 422 observed that  $C_{NO_2,L}$  is significantly influenced by  $w_{t,0}$ . For Case EX-LL, levels of  $C_{NO_2,L}$  are  
 423 extremely high (the maximum value could be up to 350 ppb). This corresponds to the lowest  $w_{t,0}$   
 424 adopted in Case EX-LL, which gives the worst (lowest) exchange between the lower and upper box  
 425 (indicated by a lower value of  $w_{t,L}$  in Figure 3). Therefore, pollutants are not efficiently carried  
 426 from the lower box to the overlying canopy layer. It is interesting to notice that the solid red curve

427 (representing the UK air quality standard for hourly  $\text{NO}_2$ ) shifts from the region with lower  
428 emissions to that with higher emissions as  $w_{t,0}$  increases. This means that even low emissions  
429 under the worst dispersion conditions can result in very poor air quality inside street canyons. It is  
430 also observed that trajectory 2005-2020 falls entirely into the region representing a breach of the  
431 UK air quality standard for hourly  $\text{NO}_2$  for Case EX-LL with the lowest  $w_{t,0}$ , for this idealised  
432 scenario. With the increase of the exchange velocity, the solid red curve moves from the year 2020  
433 towards the year 2005. It is also noted that TRES is in the region breaching the UK air quality  
434 standard for hourly  $\text{NO}_2$  for Case EX-LL, Case EX-L and Case BASE, but is within the air quality  
435 limit for Case EX-H and Case EX-HH. The detailed results along the selected lines for analysis,  
436 shown as Figure 4f, are presented below.

437 Figure 9 shows the transects of  $C_{\text{NO}_2,L}$  (ppb) for Case EX -LL, Case EX-L, Case BASE, Case EX-H  
438 and Case EX-HH through the selected lines for analysis as shown in Figure 4f. It is also observed  
439 that  $C_{\text{NO}_2,L}$  increases with the increase in  $E_{\text{VOCs}}$  and  $E_{\text{NO}_x}$ , shown as Figure 9a-c. This indicates that  
440 the control of either  $E_{\text{VOCs}}$  or  $E_{\text{NO}_x}$  is effective to reduce the  $\text{NO}_2$  levels, in the former case via  
441 repartitioning of  $\text{NO}_x$ . It is also interesting to notice that there is less change of  $C_{\text{NO}_2,L}$  where  $E_{\text{VOCs}}$   
442 is lower. The minimum and maximum differences of  $C_{\text{NO}_2,L}$  between Case EX-LL with  $w_{t,0}=0.012$   
443  $\text{m s}^{-1}$  and Case EX -HH with  $w_{t,0}=0.028 \text{ m s}^{-1}$  are 44 ppb and 201 ppb for Figure 9a, 15 ppb and  
444 136 ppb for Figure 9b, and 17 ppb and 228 ppb for Figure 9c. This indicates the importance of  
445 controlling ventilation conditions of street canyons especially for highly polluted scenarios. The  
446 direct contributions of  $\text{NO}_x$  emissions to  $C_{\text{NO}_2,L}$  for cases with different exchange velocities are  
447 represented by a series of radiating lines in Figure 9b, which indicates that photochemical processes  
448 (primarily ozone titration) contribute more to  $\text{NO}_2$  than direct emissions. It is also found that the  
449 chemically induced  $\text{NO}_2$  increases rapidly for smaller  $E_{\text{NO}_x}$  and becomes negligible for larger  $E_{\text{NO}_x}$ ,  
450 due to the limited ozone supply Figure 9d shows that  $C_{\text{NO}_2,L}$  decreases significantly with year due to  
451 the (predicted) influence of vehicle control technologies upon both  $E_{\text{VOCs}}$  and  $E_{\text{NO}_x}$ . This indicates

452 that the air quality will be improved in future years. However, for the worst ventilation condition  
453 (e.g. Case EX-LL),  $C_{NO_2,L}$  is still in the breach of the UK air quality standard for hourly  $NO_2$  over  
454 the year 2005 to 2020. This indicates that control of air ventilation together with control of vehicle  
455 emissions is important in improving air quality within street canyons. Air ventilation is strongly  
456 influenced by the urban street design and deep street canyons could lead to poor ventilation.

457 Figure 10 shows the effect of the exchange velocity ( $w_{t,0}$ ) on  $\phi_{NO_2,L}$  (%), i.e. the percentage of  
458 overestimation for  $NO_2$  in the lower canyon by the ‘one-box’ model, compared with the two-box  
459 system. It is found that  $\phi_{NO_2,L}$  decreases slightly with increasing exchange velocity ( $w_{t,0}$ ), i.e. the  
460 range of (-37.49 %, -17.64 %) among all tested emission scenarios for Case EX-LL (-35.26 %, -  
461 17.22 %) for Case EX-L, (-33.49 %, -17.07 %) for Case BASE, (-31.89 %, -17.02 %) for Case EX-  
462 H and (-30.52 %, -17.01 %) for Case EX-HH. As  $\eta = 0.5$  is adopted for all cases in Figure 10, the  
463 nonlinear patterns reflect the characteristics of scenarios with a single heterogeneity coefficient.  
464 This indicates that there is a systematic underestimation of  $NO_2$  concentrations by the ‘one-box’  
465 model and this underestimation changes significantly with the heterogeneity coefficient (Figure 4),  
466 to a much greater extent than the change with the exchange velocity (Figure 10).

467 Figure 11 illustrates the transects of  $\phi_{NO_2,L}$  (ppb) for Case EX -LL, Case EX-L, Case BASE, Case  
468 EX-H and Case EX-HH through the selected lines for analysis in Figure 4f. Figure 11a shows that  
469  $\phi_{NO_2,L}$  decreases modestly with the increase of  $E_{VOCs}$ , i.e. from -21.15 % to -26.86 % for Case EX-  
470 LL, from -19.26 % to -25.37 % for Case EX-L, from -18.14 % to -24.16 % for Case BASE, from -  
471 17.48 % to -23.16 % for Case EX-H and from -17.15 % to -22.36 % for Case EX-HH. Figure 11b  
472 shows that  $\phi_{NO_2,L}$  generally increases with the increase of  $E_{NOx}$ , except a slight decrease at  
473  $E_{NOx} / E_{TRES,NOx} = 0.2$ . Figure 11c shows that there is no significant difference between the cases  
474 with different exchange velocities (within 5 %) while both  $E_{VOCs}$  and  $E_{NOx}$  are below half of those

475 for TRES. For the emission predictions corresponding to the years 2005 to 2020 shown as Figure  
476 11d, there is also no significant change of  $\phi_{NO_2,L}$  (within 5 % difference).

### 477 **3.3 Effect of the box height ratio**

478 Figure 12 illustrates the effect of the box height ratio ( $\alpha$ ) on  $C_{NO_2,L}$  (ppb), i.e. the concentration in  
479 the lower box, for Case HB-LL ( $\alpha = 0.1$ ), (b) Case HB-L ( $\alpha = 0.3$ ), (c) Case BASE ( $\alpha = 0.5$ ), (d)  
480 Case HB-H ( $\alpha = 0.7$ ), and (e) Case HB-HH ( $\alpha = 0.9$ ). The value of  $\alpha$  can vary with the flow  
481 structure in a street canyon, which may be significantly influenced by the building geometry. A  
482 high-level circulation induced for example by a pitched building roof will give a smaller relative  
483 size of the upper vortex (Louka et al., 2000), corresponding to a higher value of  $\alpha$  (possibly  
484 equivalent to 0.9). Large eddy simulations of street canyons by Li et al. (2012) suggested that the  
485 street bottom heating may have a strong impact on the flow pattern within a deep street canyon  
486 (AR=2), i.e. the value of  $\alpha$  can about 0.44 under the neutral condition, about 0.46 under weak  
487 heating and about 0.9 under strong heating. There is clear evidence in Figure 12 that  $C_{NO_2,L}$  is  
488 significantly affected by the box height ratio. Extremely high levels of  $C_{NO_2,L}$  are observed for  
489 smaller box height ratios, e.g. with a maximum value of about 520 ppb for Case HB-LL with  $\alpha$   
490  $= 0.1$ . This small box height ratio represents the case that pollutants are essentially trapped in a low  
491 volume part of the street canyon under poor ventilation conditions. This is similar to the secondary  
492 smaller eddies near the street corner, where levels of pollutants can be extremely high. The  
493 exchange velocity between lower and upper boxes (indicated by a lower value of  $w_{t,L}$  in Figure 3) is  
494 the lowest for Case HB-LL. It is observed that almost all of the scenarios (including trajectory  
495 2005-2020) in Case HB-LL are expected to breach the UK air quality standard for hourly  $NO_2$ , for  
496 this idealised scenario, except for scenarios with extremely low emissions, shown as Figure 12a. As  
497 the box height ratio increases, the solid red curve in Figure 12 shifts towards scenarios with higher  
498 emissions across the trajectory for predicted emissions 2005-2020. For Case HB-H and Case HB-  
499 HH, the TRES falls into the region below the UK air quality standard for hourly  $NO_2$ . The box

500 height ratio is mainly determined by the flow structure in the street canyon. Therefore,  
501 understanding the flow characteristics in a street canyon is of vital importance; numerical modelling  
502 approaches can provide predictions of flow patterns at high spatial and temporal resolution within  
503 street canyons. The detailed results along the selected lines for analysis, shown as Figure 4f, are  
504 presented below.

505 Figure 13 shows the transects of  $C_{NO_2,L}$  (ppb) for Case HB-LL, Case HB-L, Case BASE, Case HB-  
506 H and Case HB-HH through the selected lines for analysis in Figure 4f. It can be seen that there is  
507 an increase of  $C_{NO_2,L}$  with the increase of  $E_{VOCs}$  and  $E_{NOx}$ . This increasing tendency is extremely  
508 significant for Case HB-LL with the lowest box height ratio ( $\alpha = 0.1$ ), i.e. 207 ppb difference for  
509 Figure 13a, 302 ppb difference for Figure 13b and 461 ppb difference for Figure 13c. For other box  
510 height ratios in Figure 13a-c, the concentration difference is around 100 ppb, much lower than that  
511 for Case HB-LL. The direct contributions of  $NO_x$  emissions to  $C_{NO_2,L}$  for cases with different box  
512 height ratios are represented by the series of radiating lines in Figure 13b, which also indicates the  
513 importance of photochemistry in converting NO to  $NO_2$ , rather than the contribution from direct  
514 emissions of  $NO_2$ . A rapid increase of the chemically induced  $NO_2$  for smaller  $E_{NOx}$  is also observed.  
515 Figure 13d shows that there is a decrease of  $C_{NO_2,L}$  with years for the corresponding predicted  
516 emissions. However, the air quality is still worse for Case HB-LL and Case HB-L, i.e. about 4  
517 times and 2 times of the UK air quality standard for hourly  $NO_2$  for the year 2005, for this idealised  
518 scenario.

519 Figure 14 shows the effect of the box height ratio ( $\alpha$ ) on  $\phi_{NO_2,L}$  (%), i.e. the percentage of  
520 overestimation for  $NO_2$  in the lower canyon, by the ‘one-box’ model. There are significant changes  
521 of  $\phi_{NO_2,L}$  with the changes of the box height ratio, i.e. (-82.22 %, -57.37 %) for Case HB-LL with  
522  $\alpha = 0.1$ , (-54.15 %, -30.26 %) for Case HB-L with  $\alpha = 0.3$ , (-33.49 %, -17.07 %) for Case BASE  
523 with  $\alpha = 0.5$ , (-17.71 %, -8.63 %) for Case HB-H with  $\alpha = 0.7$  and (-5.27 %, -2.59 %) for Case HB-  
524 HH with  $\alpha = 0.9$ . This indicates that for a higher box height ratio, the ‘one-box’ model more

525 accurately predicts  $\text{NO}_2$  concentrations, as referenced to the coupled-two-box simulation. It is also  
526 noted that  $\phi_{\text{NO}_2,L}$  is less sensitive to emissions of  $\text{NO}_x$  and VOCs when the box height ratio is  
527 higher. For the extremely high box height ratios, the upper box plays a similar role as the shear  
528 layer, where active exchange takes place. In such a situation, the two-box model can approximate to  
529 the one-box model.

530 Figure 15 illustrates the transects of  $\phi_{\text{NO}_2,L}$  (ppb) for Case HB-LL, Case HB-L, Case BASE, Case  
531 HB-H and Case HB-HH through the selected lines for analysis in Figure 4f. Figure 15a shows that  
532 the magnitude of  $\phi_{\text{NO}_2,L}$  slightly increases with the increase of  $E_{\text{VOCs}}$ , i.e. from -64.94 % to -72.29 %  
533 for  $\alpha=0.1$ , from -33.18 % to -41.62 % for  $\alpha=0.3$ , from -18.14% to -24.16 % for  $\alpha=0.5$ , from -8.98  
534 % to -12.37 % for  $\alpha=0.7$  and from -2.65 % to -3.65 % for  $\alpha=0.9$ . This indicates that the difference  
535 in  $\phi_{\text{NO}_2,L}$  decreases with an increase in the box height ratio, and the one box model performs better  
536 for the cases with a higher box height ratio. This finding is also indicated by Figure 15b, but the  
537 magnitude of  $\phi_{\text{NO}_2,L}$  slightly decreases with the increase of  $E_{\text{NO}_x}$ , especially for  $E_{\text{NO}_x} / E_{\text{TRES},\text{NO}_x}$  up to  
538 0.5. Figure 15c also shows that there is no significant change in  $\phi_{\text{NO}_2,L}$  when changing both  $E_{\text{VOCs}}$   
539 and  $E_{\text{NO}_x}$  and that  $\phi_{\text{NO}_2,L}$  is mainly influenced by the box height ratio ( $\alpha$ ). Figure 15d shows that  
540  $\phi_{\text{NO}_2,L}$  does not change significantly for the predicted emissions changes over the years 2005 to  
541 2020, but significant contrasts are found for the cases with different box height ratios.

## 542 4 Conclusions

543 The bulk levels of air pollution within a street canyon, focusing on the lower heights where  
544 pedestrian / human exposure takes place, are investigated using a coupled-two-box model approach,  
545 which enables a wide range of emission scenarios to be considered in a computationally efficient  
546 manner, whilst providing greater realism than a single, well-mixed box approach. The performance  
547 of the one-box model approach (assuming the whole street canyon as a well-mixed box) was also  
548 examined compared with the bulk concentrations in the lower canyon of the two-box model. Core



important parameters (i.e. heterogeneity coefficient, exchange velocity and box height ratio) related to the two-box model approach were investigated. The two-box model results identify the emission regimes and the meteorological conditions under which  $\text{NO}_2$  in the lower canyon (street level) is in breach of air quality standards. Higher  $\text{NO}_2$  levels were observed for the cases with higher heterogeneity coefficients (the two boxes are more segregated), or with lower exchange velocities (worse ventilation conditions) or with smaller box height ratios (reduced dilution possibly due to secondary smaller eddies in the lower canyon). The one-box model was found to systematically underestimate  $\text{NO}_2$  levels compared with those in the lower box of the two-box model for all the test scenarios. This underestimation generally tends to worsen for higher heterogeneity coefficients, lower exchange velocities, or smaller box height ratios. This study highlights the limitation of the assumption of homogeneity in single box models for street canyon simulation, and the inherent uncertainties that must be borne in mind to appropriately interpret such model output (in particular, that a single-box treatment will systematically underestimate  $\text{NO}_2$  as experienced at street level). The assumption of ‘exchange velocity’ adopted in the two-box model approach only represents the overall integrated effect of the dynamical flow between simplified street canyon boxes, failing to capture the structure of flow and pollutant distribution inside street canyons. The box model approach only provides mean concentrations within the boxes and assumes an instant and complete mixing, thus artificially augmenting chemical reaction rates within the boxes (i.e. generally enhancing the  $\text{NO}$  to  $\text{NO}_2$  conversion rate such that  $\text{NO}_2$  would be overestimated) (Zhong et al. (2015); Bright et al. (2013)). In addition, the two-box model approach (vertically segregated) is restricted to represent two vortices within a street canyon. For even taller canyons, more vortices may be formed. Future studies should adopt more photochemical boxes and use finite exchange velocities to allow an incomplete mixing across boxes (thus to be closer to the real conditions), and extend the range of scenarios to encompass the range encountered in reality. Reactive pollutant abundance could be obtained by running the two-box model if a set of parameters are provided for real urban areas as the model inputs (e.g. heterogeneity coefficient, exchange velocity, box height

ratio and emissions) although these three parameters are might be uncontrollable and site- and flow-dependent. For an application in future, it is needed to map the ‘controllable pre-defined building geometry parameters’ and meteorological conditions to the three box-model parameters we proposed in this study using available knowledge, datasets (e.g. wind tunnel experiments), and/or modelling tools (e.g. CFD). In addition, a standard procedure for setting the parameters used in the two-box model should be developed. A multi-box air quality model for a street canyon network may then be developed for practical applications.

## **Acknowledgements**

The authors would like to thank Dr Vivien Bright for provision of the reduced chemical scheme (RCS). The authors appreciate the University of Birmingham’s BlueBEAR HPC service (<http://www.bear.bham.ac.uk>) for providing the computational resource. JZ thanks the University of Birmingham for the award of a Li Siguang Scholarship, which is offered in partnership with the China Scholarship Council (CSC).

597 **Appendix A: RCS mechanism**  
598

599 **Table A1** All reactions and rate constants included in the RCS mechanism (adopted from Bright (2013)).  
600 The units of rate constants are s<sup>-1</sup> for first order reactions and ppb s<sup>-1</sup> for second order reactions. The pressure  
601 is set to 10132.5 Pa and the temperature is set to 293 K.

Reactants				Products		Rate constant
1	O <sub>3</sub>			→ OH	+ OH	3.40E-6
2	NO	+ O <sub>3</sub>	→	NO <sub>2</sub>		4.01E-4
3	NO	+ NO	→	NO <sub>2</sub>	+ NO <sub>2</sub>	2.63E-9
4	NO	+ NO <sub>3</sub>	→	NO <sub>2</sub>	+ NO <sub>2</sub>	6.56E-1
5	OH	+ O <sub>3</sub>	→	HO <sub>2</sub>		1.72E-3
6	OH	+ H <sub>2</sub>	→	HO <sub>2</sub>		1.49E-4
7	OH	+ CO	→	HO <sub>2</sub>		5.06E-3
8	H <sub>2</sub> O <sub>2</sub>	+ OH	→	HO <sub>2</sub>		4.21E-2
9	HO <sub>2</sub>	+ O <sub>3</sub>	→	OH		4.86E-5
10	OH	+ HO <sub>2</sub>	→			2.82E+0
11	HO <sub>2</sub>	+ HO <sub>2</sub>	→	H <sub>2</sub> O <sub>2</sub>		8.74E-2
12	HO <sub>2</sub>	+ HO <sub>2</sub>	→	H <sub>2</sub> O <sub>2</sub>		6.92E-2
13	OH	+ NO	→	HONO		2.54E-1
14	OH	+ NO <sub>2</sub>	→	HNO <sub>3</sub>		3.08E-1
15	OH	+ NO <sub>3</sub>	→	HO <sub>2</sub>	+ NO <sub>2</sub>	5.01E-1
16	HO <sub>2</sub>	+ NO	→	OH	+ NO <sub>2</sub>	2.27E-1
17	HO <sub>2</sub>	+ NO <sub>2</sub>	→	HO <sub>2</sub> NO <sub>2</sub>		3.59E-2
18	HO <sub>2</sub> NO <sub>2</sub>		→	HO <sub>2</sub>	+ NO <sub>2</sub>	3.74E-2
19	HO <sub>2</sub> NO <sub>2</sub>	+ OH	→	NO <sub>2</sub>		1.20E-1
20	HONO	+ OH	→	NO <sub>2</sub>		2.58E-2
21	HNO <sub>3</sub>	+ OH	→	NO <sub>3</sub>		4.08E-3
22	H <sub>2</sub> O <sub>2</sub>		→	OH	+ OH	7.11E-6
23	NO <sub>2</sub>		→	NO	+ O <sub>3</sub>	9.20E-3
24	NO <sub>3</sub>		→	NO		2.34E-2
25	NO <sub>3</sub>		→	NO <sub>2</sub>	+ O <sub>3</sub>	1.83E-1
26	HONO		→	OH	+ NO	2.02E-3

27	HNO <sub>3</sub>		→	OH	+	NO <sub>2</sub>		6.30E-7
28	CH <sub>4</sub>	+	OH	→	CH <sub>3</sub> O <sub>2</sub>			1.39E-4
29	C <sub>2</sub> H <sub>4</sub>	+	OH	→	HOCH <sub>2</sub> CH <sub>2</sub> O <sub>2</sub>			2.00E-1
30	C <sub>3</sub> H <sub>6</sub>	+	OH	→	RN <sub>9</sub> O <sub>2</sub>			7.19E-1
31	C <sub>2</sub> H <sub>4</sub>	+	O <sub>3</sub>	→	HCHO	+	CO + HO <sub>2</sub> + OH	4.46E-9
32	C <sub>2</sub> H <sub>4</sub>	+	O <sub>3</sub>	→	HCHO	+	HCOOH	2.99E-8
33	C <sub>3</sub> H <sub>6</sub>	+	O <sub>3</sub>	→	HCHO	+	CH <sub>3</sub> O <sub>2</sub> + CO + OH	8.18E-8
34	C <sub>3</sub> H <sub>6</sub>	+	O <sub>3</sub>	→	HCHO	+	CH <sub>3</sub> CO <sub>2</sub> H	1.45E-7
35	C <sub>5</sub> H <sub>8</sub>	+	OH	→	RU14O <sub>2</sub>			2.58E+0
36	C <sub>5</sub> H <sub>8</sub>	+	O <sub>3</sub>	→	UCARB10	+	CO + HO <sub>2</sub> + OH	7.76E-8
37	C <sub>5</sub> H <sub>8</sub>	+	O <sub>3</sub>	→	UCARB10	+	HCOOH	2.10E-7
38	HCHO		→	CO	+	HO <sub>2</sub> + HO <sub>2</sub>		3.05E-5
39	HCHO		→	H <sub>2</sub>	+	CO		4.61E-5
40	CH <sub>3</sub> CHO		→	CH <sub>3</sub> O <sub>2</sub>	+	HO <sub>2</sub> + CO		5.07E-6
41	HCHO	+	OH	→	HO <sub>2</sub>	+	CO	2.35E-1
42	CH <sub>3</sub> CHO	+	OH	→	CH <sub>3</sub> CO <sub>3</sub>			4.02E-1
43	CH <sub>3</sub> OH	+	OH	→	HO <sub>2</sub>	+	HCHO	2.31E-2
44	C <sub>2</sub> H <sub>5</sub> OH	+	OH	→	CH <sub>3</sub> CHO	+	HO <sub>2</sub>	7.24E-2
45	C <sub>2</sub> H <sub>5</sub> OH	+	OH	→	HOCH <sub>2</sub> CH <sub>2</sub> O <sub>2</sub>			9.23E-3
46	HCOOH	+	OH	→	HO <sub>2</sub>			1.13E-2
47	CH <sub>3</sub> CO <sub>2</sub> H	+	OH	→	CH <sub>3</sub> O <sub>2</sub>			2.00E-2
48	CH <sub>3</sub> O <sub>2</sub>	+	NO	→	HCHO	+	HO <sub>2</sub> + NO <sub>2</sub>	1.95E-1
49	HOCH <sub>2</sub> CH <sub>2</sub> O <sub>2</sub>	+	NO	→	HCHO	+	HCHO + HO <sub>2</sub> + NO <sub>2</sub>	1.68E-1
50	HOCH <sub>2</sub> CH <sub>2</sub> O <sub>2</sub>	+	NO	→	HOCH <sub>2</sub> CHO	+	HO <sub>2</sub> + NO <sub>2</sub>	4.84E-2
51	RN <sub>9</sub> O <sub>2</sub>	+	NO	→	CH <sub>3</sub> CHO	+	HCHO + HO <sub>2</sub> + NO <sub>2</sub>	2.13E-1
52	CH <sub>3</sub> CO <sub>3</sub>	+	NO	→	CH <sub>3</sub> O <sub>2</sub>	+	NO <sub>2</sub>	5.10E-1
53	HOCH <sub>2</sub> CO <sub>3</sub>	+	NO	→	HO <sub>2</sub>	+	HCHO + NO <sub>2</sub>	5.10E-1
54	RU14O <sub>2</sub>	+	NO	→	UCARB12	+	HO <sub>2</sub> + NO <sub>2</sub>	4.93E-2
55	RU14O <sub>2</sub>	+	NO	→	UCARB10	+	HCHO + HO <sub>2</sub> + NO <sub>2</sub>	1.46E-1
56	RU12O <sub>2</sub>	+	NO	→	CH <sub>3</sub> CO <sub>3</sub>	+	HOCH <sub>2</sub> CHO + NO <sub>2</sub>	1.52E-1
57	RU12O <sub>2</sub>	+	NO	→	CARB7	+	CO + HO <sub>2</sub> + NO <sub>2</sub>	6.52E-2
58	RU10O <sub>2</sub>	+	NO	→	CH <sub>3</sub> CO <sub>3</sub>	+	HOCH <sub>2</sub> CHO + NO <sub>2</sub>	1.09E-1

59	RU10O <sub>2</sub>	+	NO	→	CARB6	+	HCHO	+	HO <sub>2</sub>	+	NO <sub>2</sub>	6.52E-2
60	RU10O <sub>2</sub>	+	NO	→	CARB7	+	HCHO	+	HO <sub>2</sub>	+	NO <sub>2</sub>	4.35E-2
61	CH <sub>3</sub> O <sub>2</sub>	+	NO	→	CH <sub>3</sub> NO <sub>3</sub>							1.95E-4
62	HOCH <sub>2</sub> CH <sub>2</sub> O <sub>2</sub>	+	NO	→	HOC <sub>2</sub> H <sub>4</sub> NO <sub>3</sub>							1.09E-3
63	RN <sub>9</sub> O <sub>2</sub>	+	NO	→	RN9NO <sub>3</sub>							4.56E-3
64	RU14O <sub>2</sub>	+	NO	→	RU14NO <sub>3</sub>							2.17E-2
65	CH <sub>3</sub> O <sub>2</sub>	+	HO <sub>2</sub>	→	CH <sub>3</sub> OOH							1.52E-1
66	HOCH <sub>2</sub> CH <sub>2</sub> O <sub>2</sub>	+	HO <sub>2</sub>	→	HOC <sub>2</sub> H <sub>4</sub> OOH							3.62E-1
67	RN9O <sub>2</sub>	+	HO <sub>2</sub>	→	RN9OOH							3.20E-1
68	CH <sub>3</sub> CO <sub>3</sub>	+	HO <sub>2</sub>	→	CH <sub>3</sub> CO <sub>3</sub> H							3.75E-1
69	HOCH <sub>2</sub> CO <sub>3</sub>	+	HO <sub>2</sub>	→	HOCH <sub>2</sub> CO <sub>3</sub> H							3.75E-1
70	RU14O <sub>2</sub>	+	HO <sub>2</sub>	→	RU14OOH							4.74E-1
71	RU12O <sub>2</sub>	+	HO <sub>2</sub>	→	RU12OOH							4.35E-1
72	RU10O <sub>2</sub>	+	HO <sub>2</sub>	→	RU10OOH							3.85E-1
73	CH <sub>3</sub> O <sub>2</sub>			→	HCHO	+	HO <sub>2</sub>					6.22E-3*
74	CH <sub>3</sub> O <sub>2</sub>			→	HCHO							6.32E-3*
75	CH <sub>3</sub> O <sub>2</sub>			→	CH <sub>3</sub> OH							6.32E-3*
76	HOCH <sub>2</sub> CH <sub>2</sub> O <sub>2</sub>			→	HOCH <sub>2</sub> CHO	+	HO <sub>2</sub>					1.12E-2*
77	RN9O <sub>2</sub>			→	CH <sub>3</sub> CHO	+	HCHO	+	HO <sub>2</sub>			2.20E-2*
78	CH <sub>3</sub> CO <sub>3</sub>			→	CH <sub>3</sub> O <sub>2</sub>							2.50E-1*
79	HOCH <sub>2</sub> CO <sub>3</sub>			→	HCHO	+	HO <sub>2</sub>					2.50E-1*
80	RU14O <sub>2</sub>			→	UCARB12	+	HO <sub>2</sub>					1.08E-2*
81	RU14O <sub>2</sub>			→	UCARB10	+	HCHO	+	HO <sub>2</sub>			3.20E-2*
82	RU12O <sub>2</sub>			→	CH <sub>3</sub> CO <sub>3</sub>	+	HOCH <sub>2</sub> CHO					3.51E-2*
83	RU12O <sub>2</sub>			→	CARB7	+	HOCH <sub>2</sub> CHO	+	HO <sub>2</sub>			1.50E-2*
84	RU10O <sub>2</sub>			→	CH <sub>3</sub> CO <sub>3</sub>	+	HOCH <sub>2</sub> CHO					2.50E-2*
85	RU10O <sub>2</sub>			→	CARB6	+	HCHO	+	HO <sub>2</sub>			1.50E-2*
86	RU10O <sub>2</sub>			→	CARB7	+	HCHO	+	HO <sub>2</sub>			1.00E-2*
87	CARB7			→	CH <sub>3</sub> CO <sub>3</sub>	+	HCHO	+	HO <sub>2</sub>			3.36E-6
88	HOCH <sub>2</sub> CHO			→	HCHO	+	CO	+	HO <sub>2</sub>	+	HO <sub>2</sub>	1.77E-5
89	UCARB10			→	CH <sub>3</sub> CO <sub>3</sub>	+	HCHO	+	HO <sub>2</sub>			1.62E-5
90	CARB6			→	CH <sub>3</sub> CO <sub>3</sub>	+	CO	+	HO <sub>2</sub>			1.26E-4

91	UCARB12		→	CH <sub>3</sub> CO <sub>3</sub>	+	HOCH2CHO	+	CO	+	HO2	1.62E-5	
92	CARB7	+	OH	→	CARB6	+	HO <sub>2</sub>				7.51E-2	
93	UCARB10	+	OH	→	RU10O <sub>2</sub>						6.26E-1	
94	UCARB10	+	O <sub>3</sub>	→	HCHO	+	CH <sub>3</sub> CO <sub>3</sub>	+	CO	+	OH	4.21E-8
95	UCARB10	+	O <sub>3</sub>	→	HCHO	+	CARB6	+	H <sub>2</sub> O <sub>2</sub>			2.93E-8
96	HOCH <sub>2</sub> CHO	+	OH	→	HOCH <sub>2</sub> CO <sub>3</sub>							2.50E-1
97	CARB6	+	OH	→	CH <sub>3</sub> CO <sub>3</sub>	+	CO					4.31E-1
98	UCARB12	+	OH	→	RU12O <sub>2</sub>							1.13E-0
99	UCARB12	+	O <sub>3</sub>	→	HOCH <sub>2</sub> CHO	+	CH <sub>3</sub> CO <sub>3</sub>	+	CO	+	OH	5.35E-7
100	UCARB12	+	O <sub>3</sub>	→	HOCH <sub>2</sub> CHO	+	CARB6	+	H <sub>2</sub> O <sub>2</sub>			6.61E-8
101	CH <sub>3</sub> NO <sub>3</sub>		→	HCHO	+	HO <sub>2</sub>	+	NO <sub>2</sub>				8.96E-7
102	CH <sub>3</sub> NO <sub>3</sub>	+	OH	→	HCHO	+	NO <sub>2</sub>					9.33E-3
103	HOC <sub>2</sub> H <sub>4</sub> NO <sub>3</sub>	+	OH	→	HOCH <sub>2</sub> CHO	+	NO <sub>2</sub>					2.73E-2
104	RN9NO <sub>3</sub>	+	OH	→	CARB7	+	NO <sub>2</sub>					3.28E-2
105	RU14NO <sub>3</sub>	+	OH	→	UCARB12	+	NO <sub>2</sub>					1.39E+0
106	CH <sub>3</sub> OOH		→	HCHO	+	HO <sub>2</sub>	+	OH				5.44E-6
107	CH <sub>3</sub> CO <sub>3</sub> H		→	CH <sub>3</sub> O <sub>2</sub>	+	OH						5.44E-6
108	HOCH <sub>2</sub> CO <sub>3</sub> H		→	HCHO	+	HO <sub>2</sub>	+	OH				5.44E-6
109	RU14OOH		→	UCARB12	+	HO <sub>2</sub>	+	OH				1.37E-6
110	RU14OOH		→	UCARB10	+	HCHO	+	HO <sub>2</sub>	+	OH		4.07E-6
111	RU12OOH		→	CARB6	+	HOCH2CHO	+	HO <sub>2</sub>	+	OH		5.44E-6
112	RU10OOH		→	CH <sub>3</sub> CO <sub>3</sub>	+	HOCH2CHO	+	OH				5.44E-6
113	HOC <sub>2</sub> H <sub>4</sub> OOH		→	HCHO	+	HCHO	+	HO <sub>2</sub>	+	OH		5.44E-6
114	RN9OOH		→	CH <sub>3</sub> CHO	+	HCHO	+	HO <sub>2</sub>	+	OH		5.44E-6
115	CH <sub>3</sub> OOH	+	OH	→	CH <sub>3</sub> O <sub>2</sub>							9.10E-1
116	CH <sub>3</sub> OOH	+	OH	→	HCHO	+	OH					4.79E-1
117	CH <sub>3</sub> CO <sub>3</sub> H	+	OH	→	CH <sub>3</sub> CO <sub>3</sub>							9.27E-2
118	HOCH <sub>2</sub> CO <sub>3</sub> H	+	OH	→	HOCH <sub>2</sub> CO <sub>3</sub>							1.55E-1
119	RU14OOH	+	OH	→	UCARB12	+	OH					1.88E+0
120	RU12OOH	+	OH	→	RU12O <sub>2</sub>							7.51E-1
121	RU10OOH	+	OH	→	RU10O <sub>2</sub>							7.51E-1
122	HOC <sub>2</sub> H <sub>4</sub> OOH	+	OH	→	HOCH <sub>2</sub> CHO	+	OH					5.34E-1

123	RN9OOH	+	OH	→	CARB7	+	OH		6.26E-1
124	CH <sub>3</sub> CO <sub>3</sub>	+	NO <sub>2</sub>	→	PAN				2.68E-1
125	PAN			→	CH <sub>3</sub> CO <sub>3</sub>	+	NO <sub>2</sub>		1.51E-4
126	HOCH <sub>2</sub> CO <sub>3</sub>	+	NO <sub>2</sub>	→	PHAN				2.68E-1
127	PHAN			→	HOCH <sub>2</sub> CO <sub>3</sub>	+	NO <sub>2</sub>		1.51E-4
128	PAN	+	OH	→	HCHO	+	CO	+	NO <sub>2</sub>
129	PHAN	+	OH	→	HCHO	+	CO	+	NO <sub>2</sub>
130	RU12O <sub>2</sub>	+	NO <sub>2</sub>	→	RU12PAN				1.63E-2
131	RU12PAN			→	RU12O <sub>2</sub>	+	NO <sub>2</sub>		1.51E-4
132	RU10O <sub>2</sub>	+	NO <sub>2</sub>	→	MPAN				1.10E-2
133	MPAN			→	RU10O <sub>2</sub>	+	NO <sub>2</sub>		1.51E-4
134	MPAN	+	OH	→	CARB7	+	CO	+	NO <sub>2</sub>
135	RU12PAN	+	OH	→	UCARB10	+	NO <sub>2</sub>		6.31E-1
136	NO <sub>2</sub>	+	O <sub>3</sub>	→	NO <sub>3</sub>				7.65E-7

Note: \* means peroxy radical summation, which is applied to the RO<sub>2</sub> permutation reactions.

[RO<sub>2</sub>] = [CH<sub>3</sub>O<sub>2</sub>] + [HOCH<sub>2</sub>CH<sub>2</sub>O<sub>2</sub>] + [RN9O<sub>2</sub>] + [CH<sub>3</sub>CO<sub>3</sub>] + [HOCH<sub>2</sub>CO<sub>3</sub>] + [RU14O<sub>2</sub>] + [RU12O<sub>2</sub>] + [RU10O<sub>2</sub>]

602

603

604

605

606

607

608

609

610

611

612      **Table 1 Overview of the model scenarios**

Case	Heterogeneity coefficient ( $\eta$ )	Exchange velocity $w_{t,0}$ ( $\text{m s}^{-1}$ )	Box height ratio ( $\alpha$ )
BASE	0.5	0.02	0.5
HC-LL	0.1	0.02	0.5
HC-L	0.3	0.02	0.5
HC-H	0.7	0.02	0.5
HC-HH	0.9	0.02	0.5
EX-LL	0.5	0.012	0.5
EX-L	0.5	0.016	0.5
EX-H	0.5	0.024	0.5
EX-HH	0.5	0.028	0.5
BH-LL	0.5	0.02	0.1
BH-L	0.5	0.02	0.3
BH-H	0.5	0.02	0.7
BH-H	0.5	0.02	0.9
Note: ‘BASE’ is the base case. ‘HC’ denotes the heterogeneity coefficient; ‘EX’ denotes the exchange velocity; ‘BH’ denotes the box height ratio. ‘LL’, ‘L’, ‘H’ and ‘HH’ represent a even lower, lower, higher and even higher value than the corresponding component in the case BASE, respectively.			

613

614

615

616

617

618

619

620

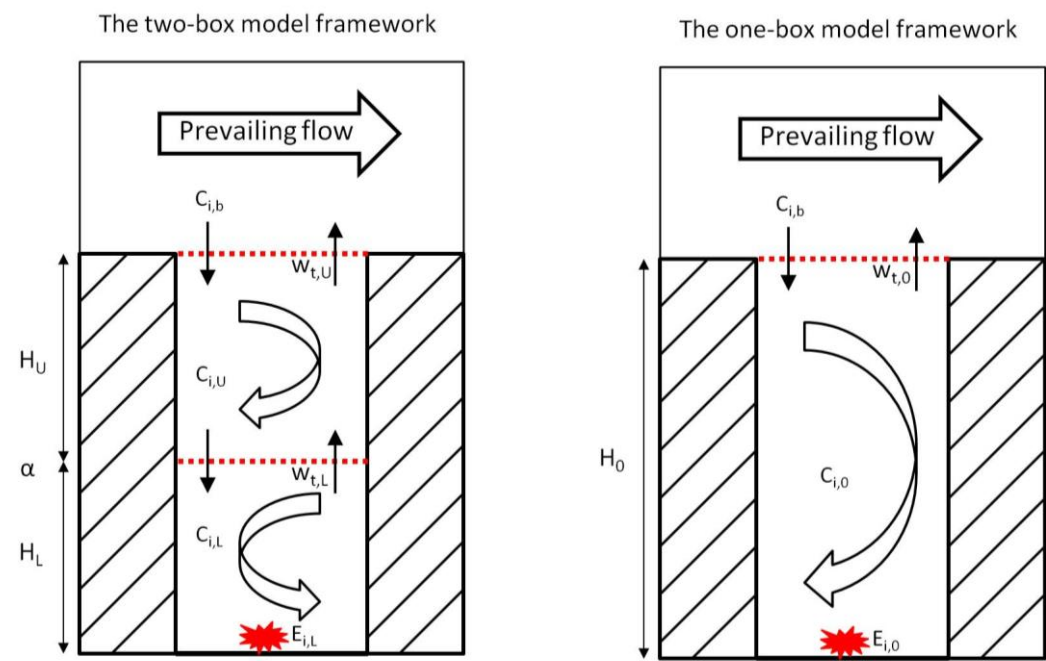
621



622

(a)

(b)



623

624 **Figure 1 Framework of the coupled two-box and one-box models (see text for details).**

625

626

627

628

629

630

631

632

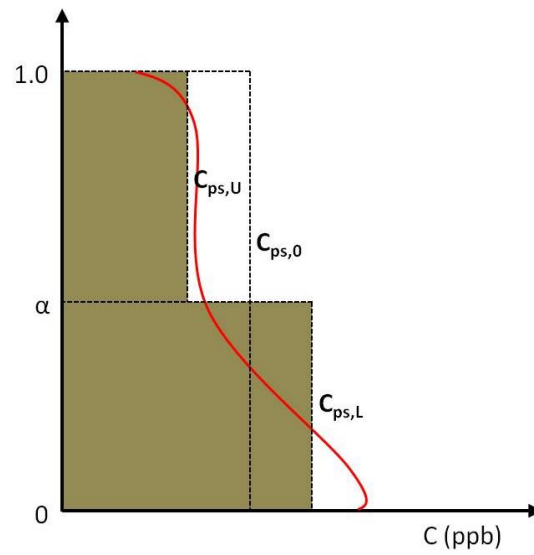
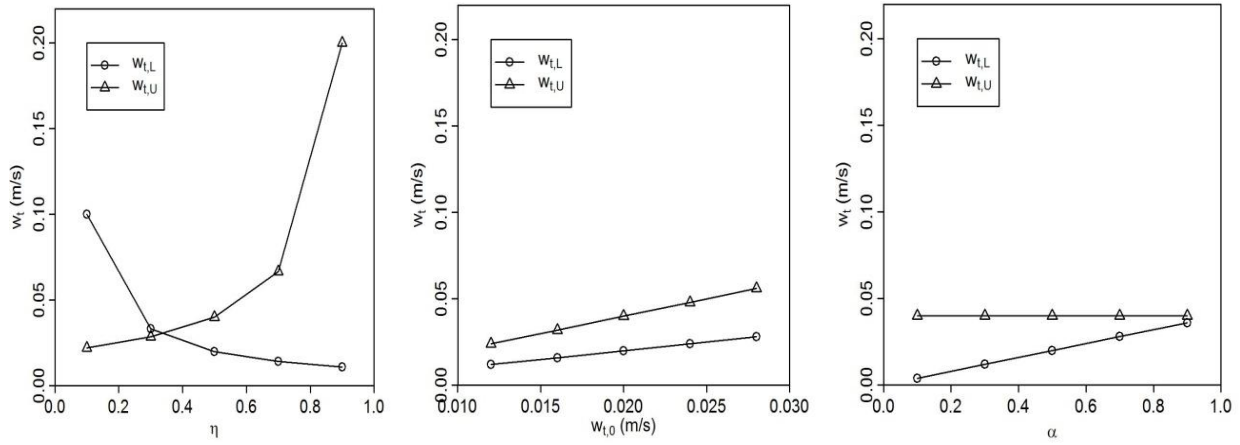


**Figure 2 Schematic diagram of the vertical concentration profile and bulk concentrations in the lower and upper boxes, and in the whole street canyon of passive scalar.**

650 (a) (b) (c)

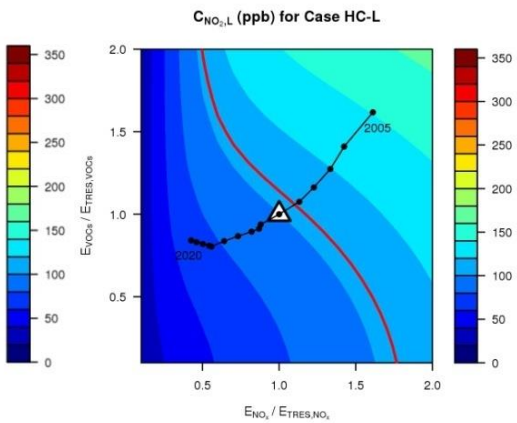
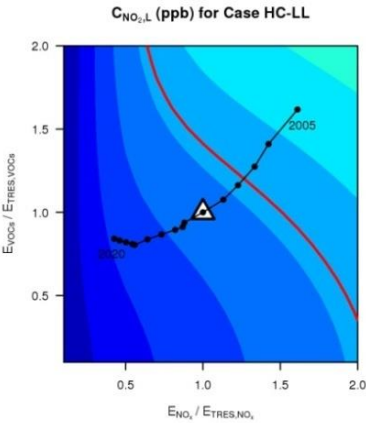


651  
652 **Figure 3** The relationship between exchange velocities for the two-box model against (a)  $\eta$  when  $\alpha = 0.5$ , (b)  
653  $w_{t,0}$  when  $\alpha = 0.5$  and  $\eta = 0.5$ , and (c)  $\alpha$  when  $\eta = 0.5$  and  $w_{t,0} = 0.02$  (m s<sup>-1</sup>). See Equations 13-14.

666

(a)

(b)

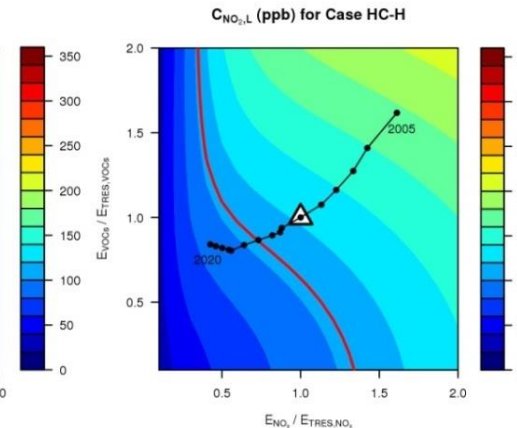
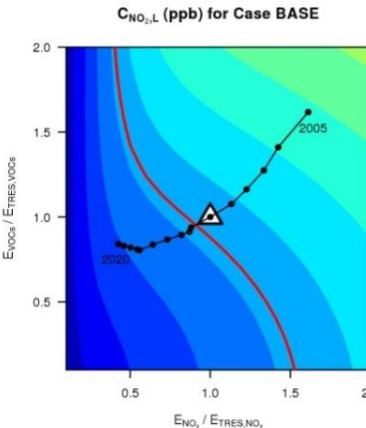


667

668

(c)

(d)

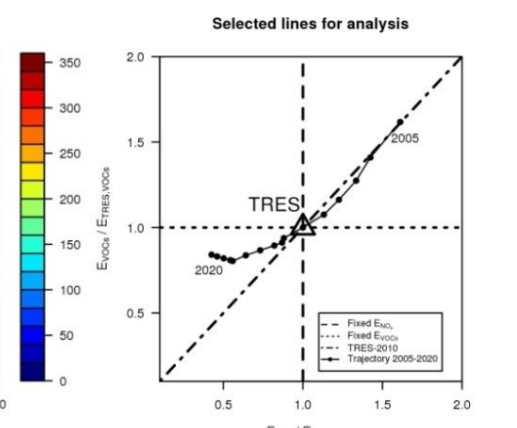
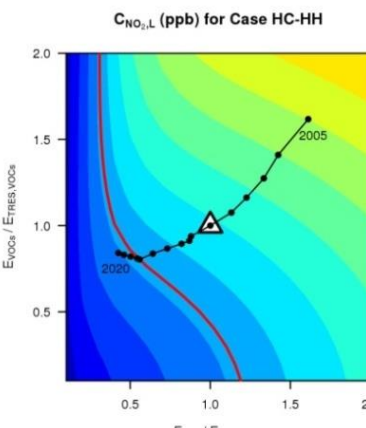


669

670

(e)

(f)



671

672

673

674

675

676

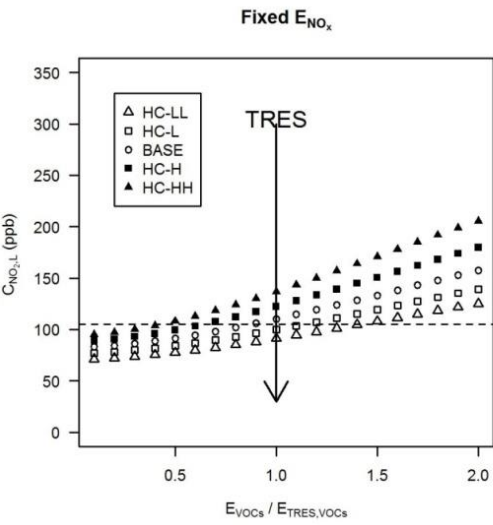
677

678

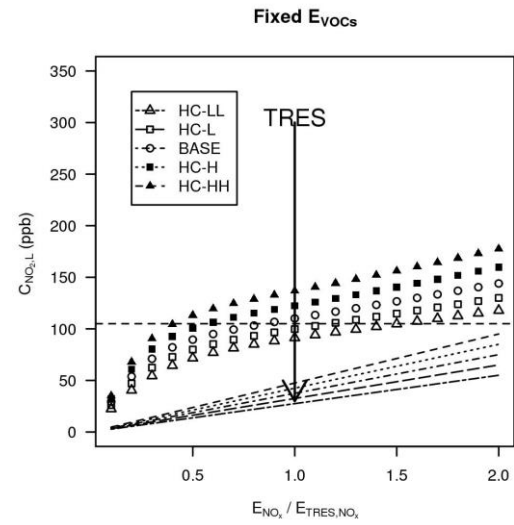
**Figure 4**  $C_{NO_2,L}$  (ppb), i.e. the concentration in the lower box derived from the “two-box” model, in the (a) Case HC-LL ( $\eta=0.1$ ), (b) Case HC-L ( $\eta=0.3$ ), (c) Case BASE ( $\eta=0.5$ ), (d) Case HC-H ( $\eta=0.7$ ), (e) Case HC-HH ( $\eta=0.9$ ) and (f) Selected lines for analysis.  $E_{VOCs}$  and  $E_{NOx}$  are normalised by those of the Typical Real-world Emission Scenario (TRES, represented by  $\Delta$ ), for the year of 2010. Trajectory 2005-2020 represents the emission scenarios for 2005 to 2020, assuming constant traffic volume and speed. The solid red curves denote the UK air quality standard for hourly  $NO_2$  (105 ppb).

679

(a)



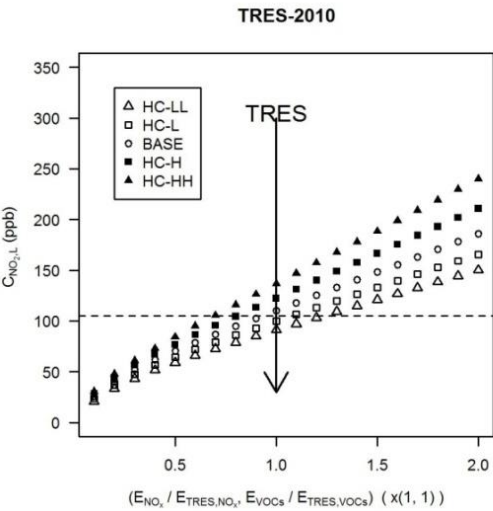
(b)



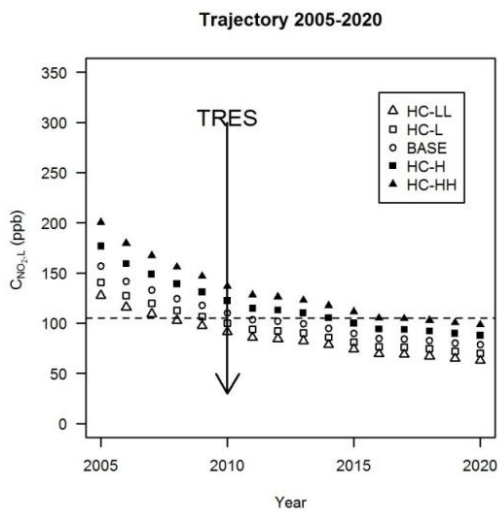
680

681

(c)



(d)



682

683

684

685

686

687

688

689

690

691

692

693

694

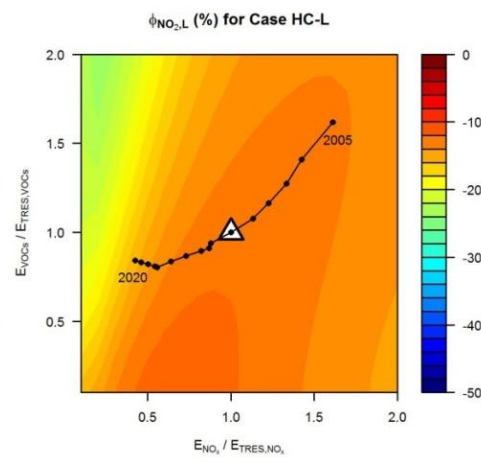
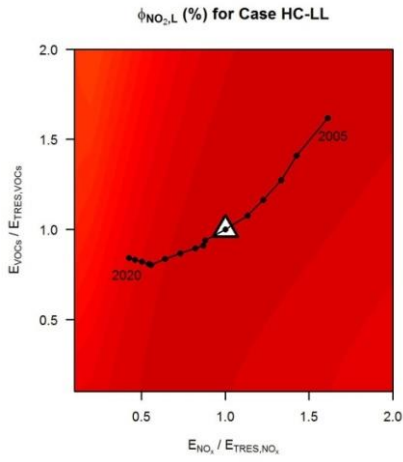
695

**Figure 5**  $C_{NO_2,L}$  (ppb), i.e. the concentration in the lower box derived from the “two-box” model, for (a) “Fixed  $E_{NO_x}$ ” at a fixed  $NO_x$  emissions of TRES, (b) “Fixed  $E_{VOCs}$ ” at a fixed  $VOCs$  emissions of TRES (The direct contributions of  $NO_x$  emissions to  $C_{NO_2,L}$  are indicated by a series of radiating lines, running from highest to lowest for the cases from HC-HH to HC-LL.), (c) “TRES-2010” varying the total traffic volume only and (d) “Trajectory 2005-2020” assuming constant traffic volume and speed varying  $\eta$ .  $E_{VOCs}$  and  $E_{NO_x}$  are normalised by those of the Typical Real-world Emission Scenario (TRES, represented by  $\Delta$ ), for the year of 2010. The dashed line indicates the UK air quality standard for hourly  $NO_2$  (105 ppb).

696

(a)

(b)

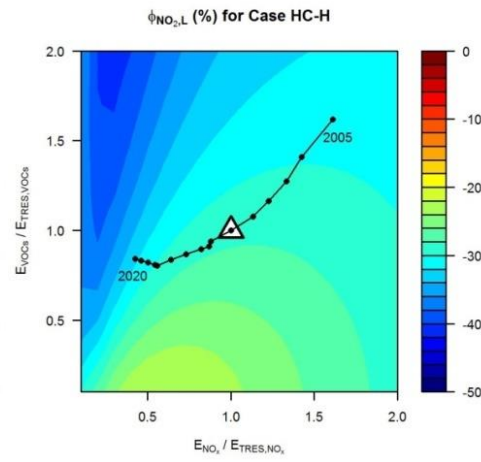
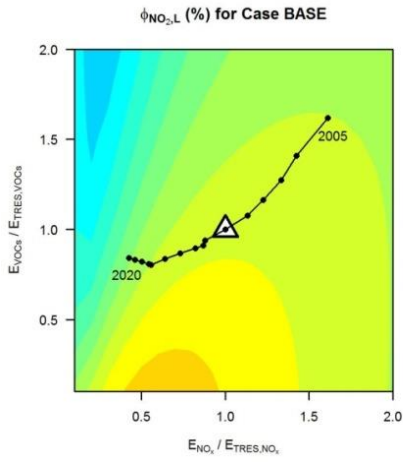


697

698

(c)

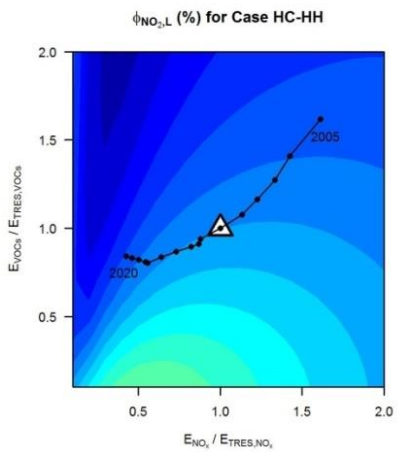
(d)



699

700

(e)



701

702

703

704

705

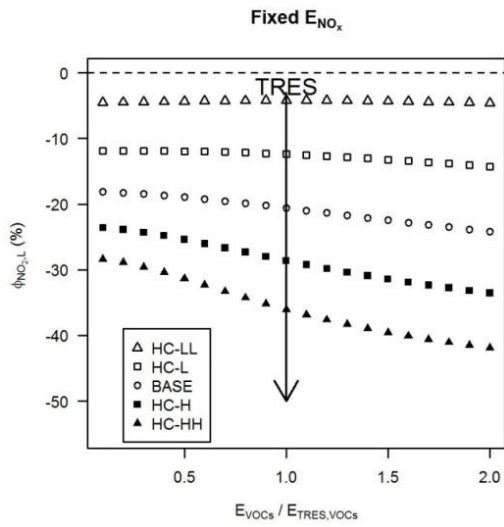
706

**Figure 6**  $\phi_{NO_2,L}$  (%), i.e. the percentage of overestimation for  $NO_2$  in the lower canyon by the ‘one-box’ model compared with that by the “two-box” model, in the (a) Case HC-LL ( $\eta=0.1$ ), (b) Case HC-L ( $\eta=0.3$ ), (c) Case BASE ( $\eta=0.5$ ), (d) Case HC-H ( $\eta=0.7$ ), (e) Case HC-HH ( $\eta=0.9$ ).  $E_{VOCs}$  and  $E_{NOx}$  are normalised by those of the Typical Real-world Emission Scenario (TRES, represented by  $\triangle$ ), for the year of 2010. Trajectory 2005-2020 represents the emission scenarios for 2005 to 2020, assuming constant traffic volume and speed.

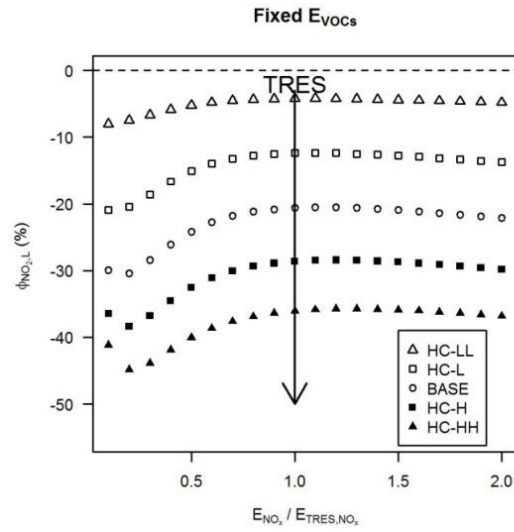
707

708

(a)



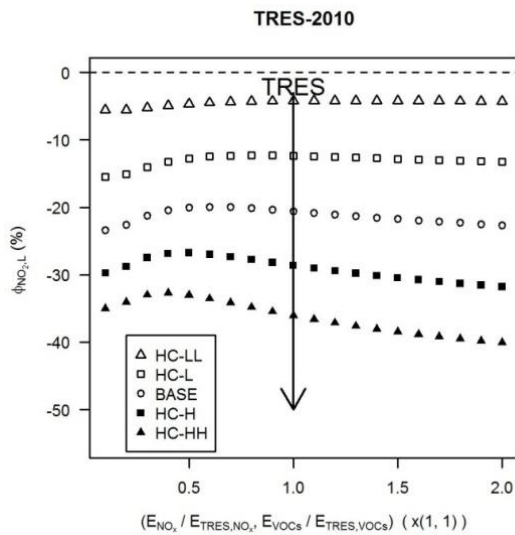
(b)



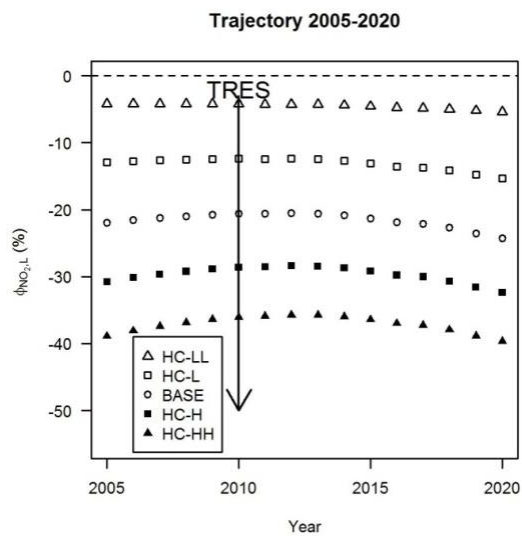
709

710

(c)



(d)



711

712

713

714

715

716

717

718

719

720

721

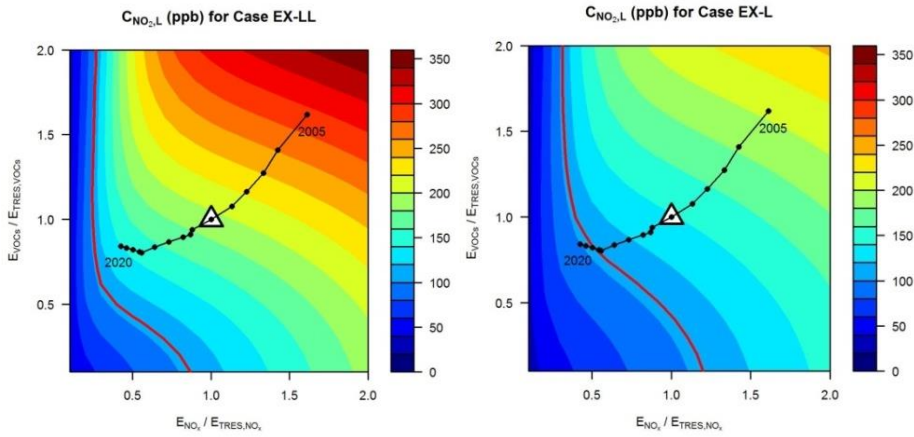
**Figure 7**  $\phi_{NO_2,L}$  (%), i.e. the percentage of overestimation for  $NO_2$  in the lower canyon by the ‘one-box’ model compared with that by the “two-box” model, for (a) “Fixed  $E_{NOx}$ ” at a fixed  $NO_x$  emissions of TRES, (b) “Fixed  $E_{VOCs}$ ” at a fixed  $VOCs$  emissions of TRES, (c) “TRES-2010” varying the total traffic volume only and (d) “Trajectory 2005-2020” assuming constant traffic volume and speed varying  $\eta$ .  $E_{VOCs}$  and  $E_{NOx}$  are normalised by those of the Typical Real-world Emission Scenario (TRES, represented by  $\Delta$ ), for the year of 2010.



722

(a)

(b)

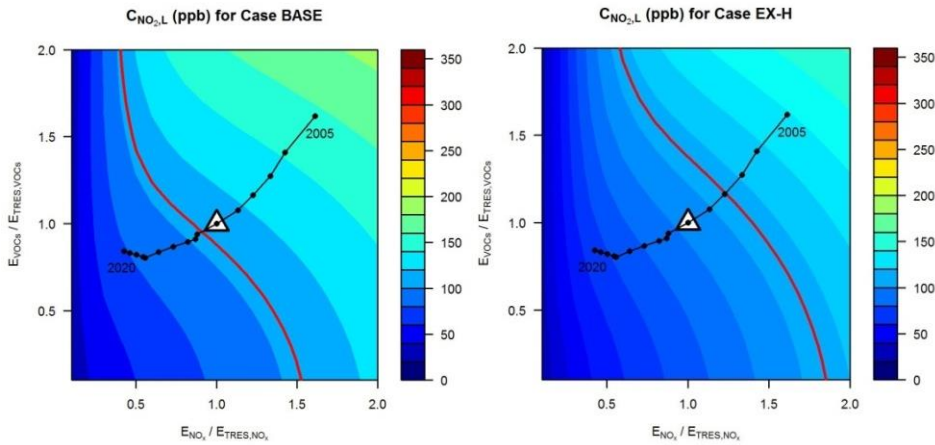


723

724

(c)

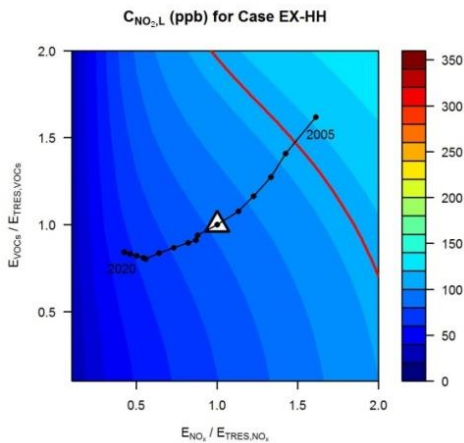
(d)



725

726

(e)



727

728

729

730

731

732

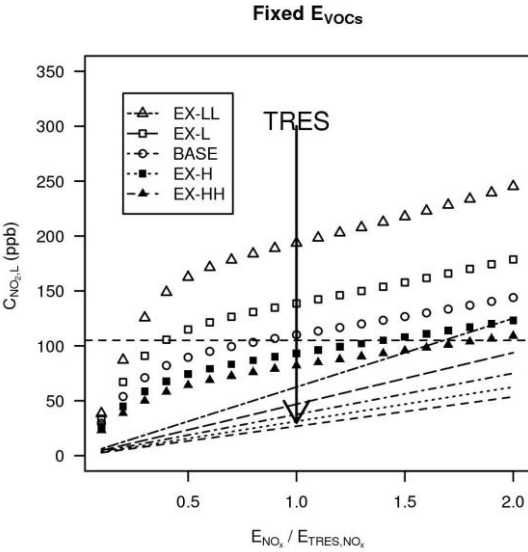
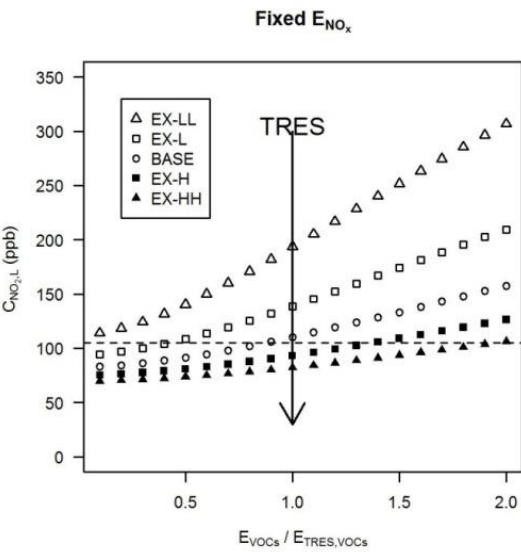
733

**Figure 8**  $C_{NO_2,L}$  (ppb), i.e. the concentration in the lower box derived from the “two-box” model, in the (a) Case EX-LL ( $w_{t,0} = 0.012 \text{ m s}^{-1}$ ), (b) Case EX-L ( $w_{t,0} = 0.016 \text{ m s}^{-1}$ ), (c) Case BASE ( $w_{t,0} = 0.02 \text{ m s}^{-1}$ ), (d) Case EX-H ( $w_{t,0} = 0.024 \text{ m s}^{-1}$ ) and (e) Case EX-HH ( $w_{t,0} = 0.028 \text{ m s}^{-1}$ ).  $E_{VOCs}$  and  $E_{NOx}$  are normalised by those of the Typical Real-world Emission Scenario (TRES, represented by  $\triangle$ ), for the year of 2010. Trajectory 2005-2020 represents the emission scenarios for 2005 to 2020, assuming constant traffic volume and speed. The solid red curves denote the UK air quality standard for hourly  $NO_2$  (105 ppb).



734

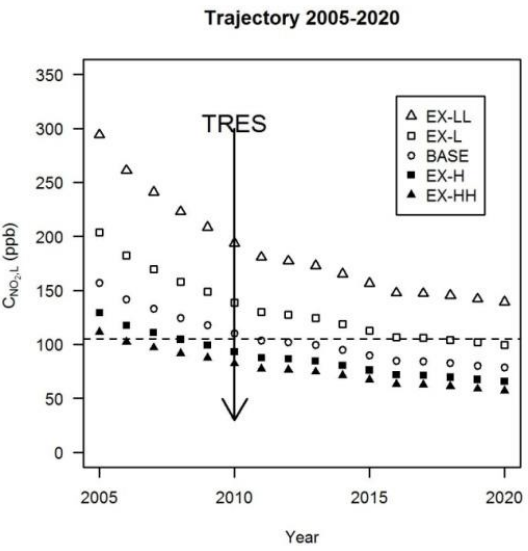
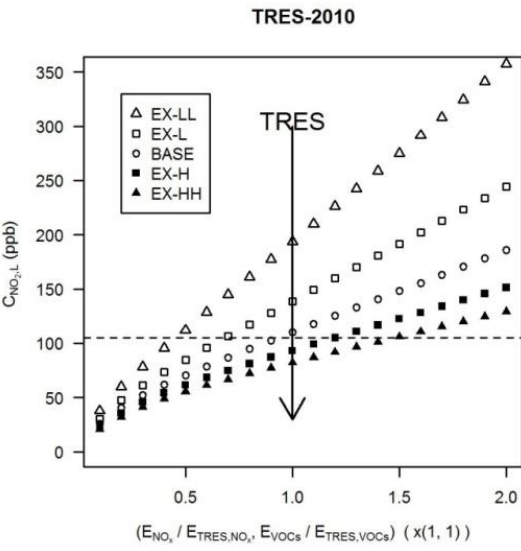
(a) (b)



735

736

(c) (d)



737

738

739

740

741

742

743

744

745

746

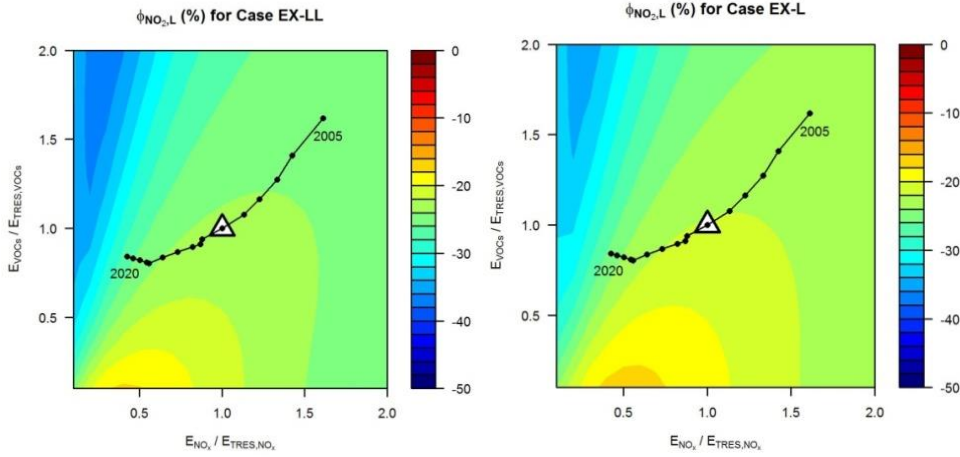
747

**Figure 9**  $C_{NO_2,L}$  (ppb), i.e. the concentration in the lower box derived from the “two-box” model, for (a) “Fixed  $E_{NOx}$ ” at a fixed  $NO_x$  emissions of TRES, (b) “Fixed  $E_{VOCs}$ ” at a fixed  $VOCs$  emissions of TRES (The direct contributions of  $NO_x$  emissions to  $C_{NO_2,L}$  are indicated by a series of radiating lines, running from highest to lowest for the cases from EX-LL to HC-HH.), (c) “TRES-2010” varying the total traffic volume only and (d) “Trajectory 2005-2020” assuming constant traffic volume and speed varying  $w_{t,0} \cdot E_{VOCs}$  and  $E_{NOx}$  are normalised by those of the Typical Real-world Emission Scenario (TRES, represented by  $\Delta$ ), for the year of 2010. The dashed line indicates the UK air quality standard for hourly  $NO_2$  (105 ppb).

748

(a)

(b)

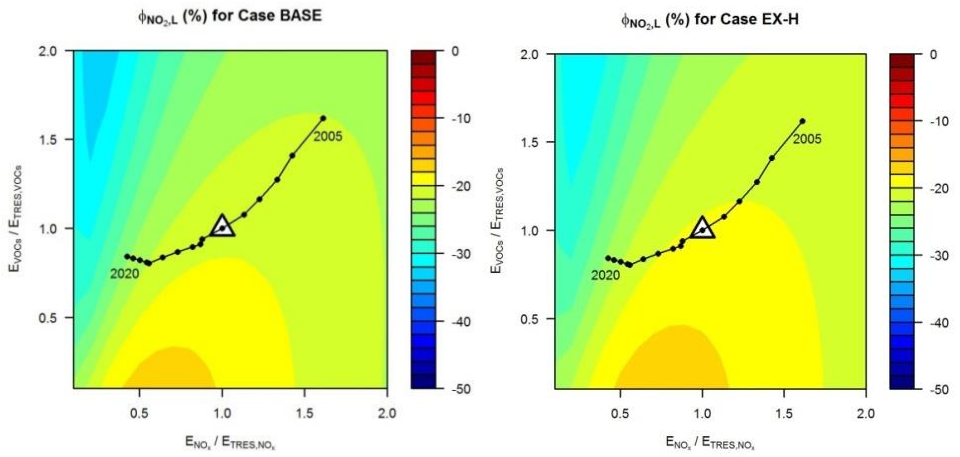


749

750

(c)

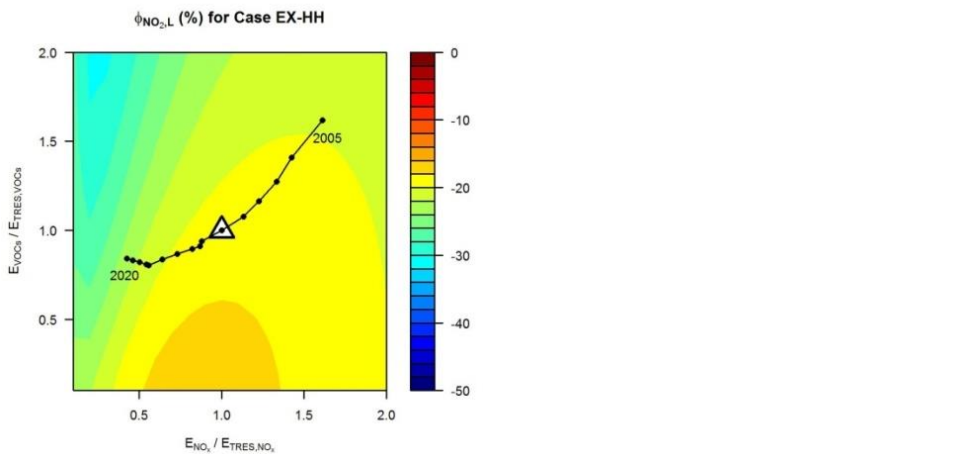
(d)



751

752

(e)



753

754

755

756

757

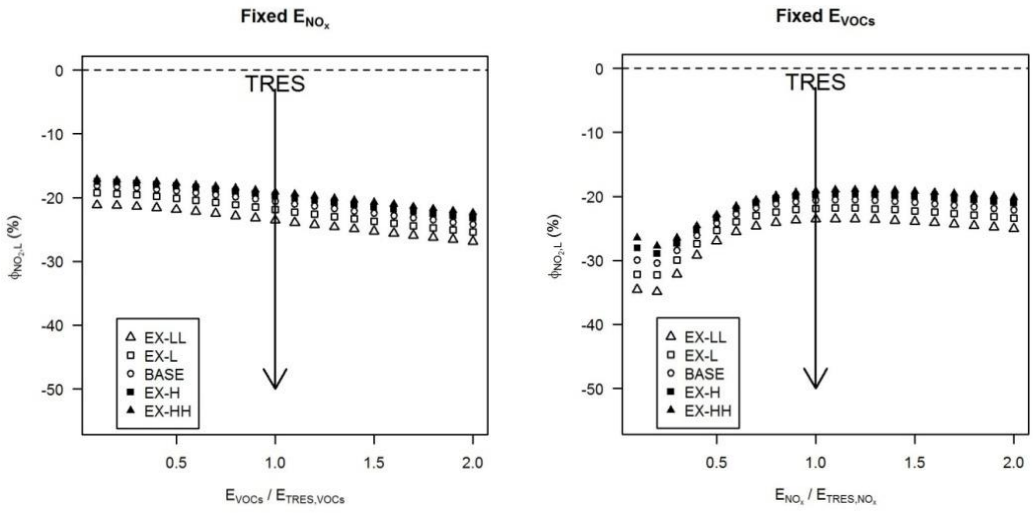
758

759

**Figure 10**  $\phi_{NO_2,L}$  (%), i.e. the percentage of overestimation for  $NO_2$  in the lower canyon by the ‘one-box’ model compared with that by the “two-box” model, in the (a) Case EX-LL ( $w_{t,0} = 0.012 \text{ m s}^{-1}$ ), (b) Case EX-L ( $w_{t,0} = 0.016 \text{ m s}^{-1}$ ), (c) Case BASE ( $w_{t,0} = 0.02 \text{ m s}^{-1}$ ), (d) Case EX-H ( $w_{t,0} = 0.024 \text{ m s}^{-1}$ ) and (e) Case EX-HH ( $w_{t,0} = 0.028 \text{ m s}^{-1}$ ).  $E_{VOCS}$  and  $E_{NOx}$  are normalised by those of the Typical Real-world Emission Scenario (TRES, represented by  $\Delta$ ), for the year of 2010. Trajectory 2005-2020 represents the emission scenarios for 2005 to 2020, assuming constant traffic volume and speed.

760

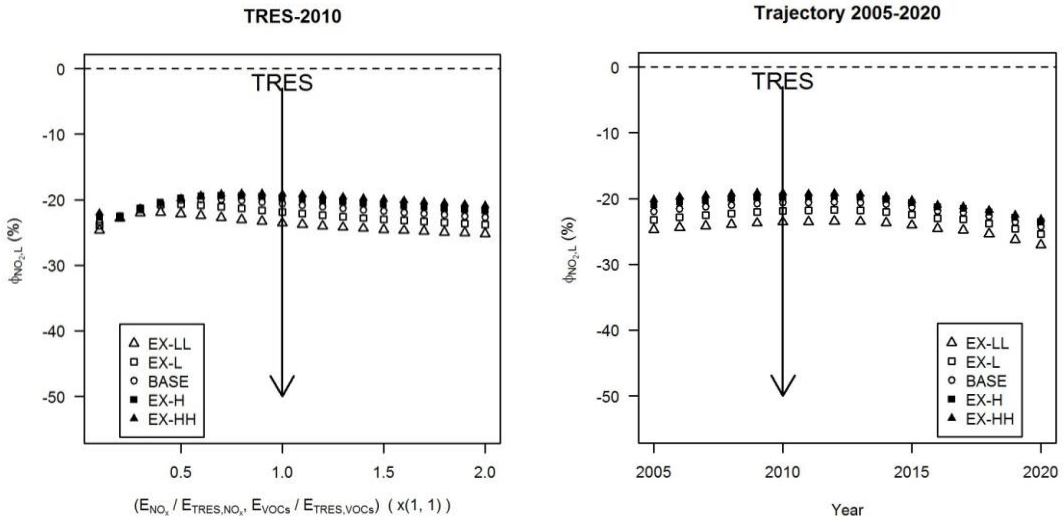
(a) (b)



761

762

(c) (d)



763

764

765

766

767

768

769

770

771

772

773

774

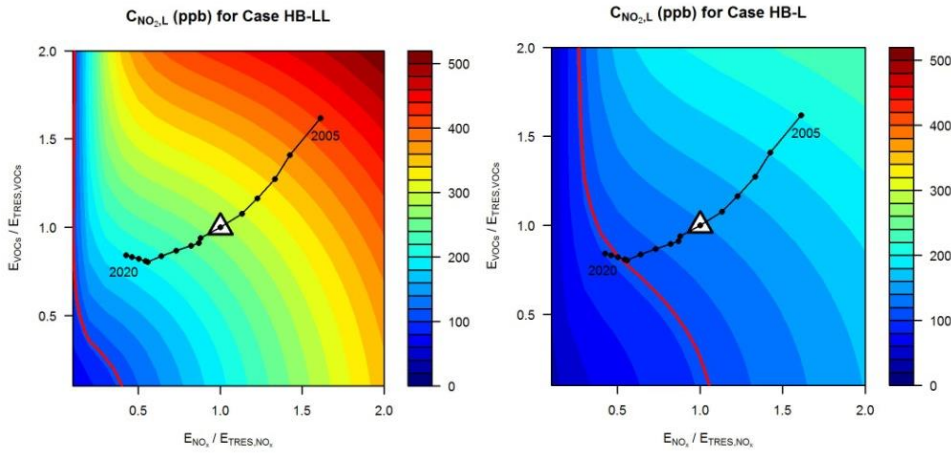
**Figure 11**  $\phi_{NO_2,L}$  (%), i.e. the percentage of overestimation for  $NO_2$  in the lower canyon by the ‘one-box’ model compared with that by the “two-box” model, for (a) “Fixed  $E_{NOx}$ ” at a fixed  $NO_x$  emissions of TRES, (b) “Fixed  $E_{VOCs}$ ” at a fixed  $VOCs$  emissions of TRES, (c) “TRES-2010” varying the total traffic volume only and (d) “Trajectory 2005-2020” assuming constant traffic volume and speed varying  $w_{t,0}$ .  $E_{VOCs}$  and  $E_{NOx}$  are normalised by those of the Typical Real-world Emission Scenario (TRES, represented by  $\Delta$ ), for the year of 2010.

775

776

(a)

(b)

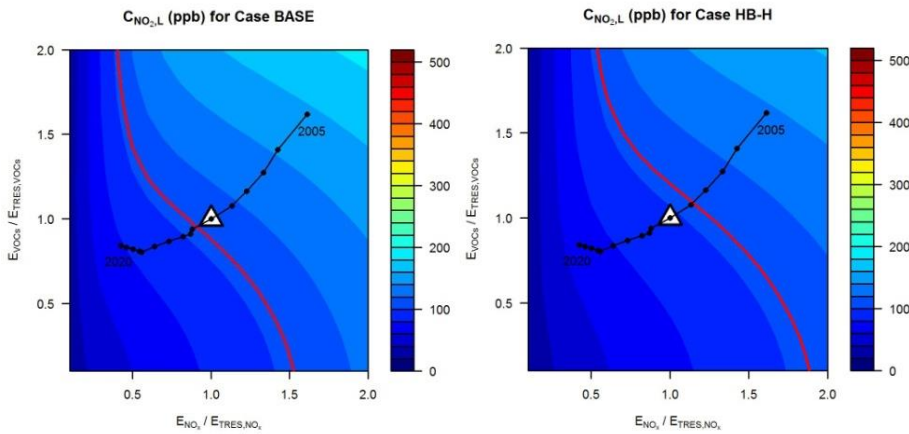


777

778

(c)

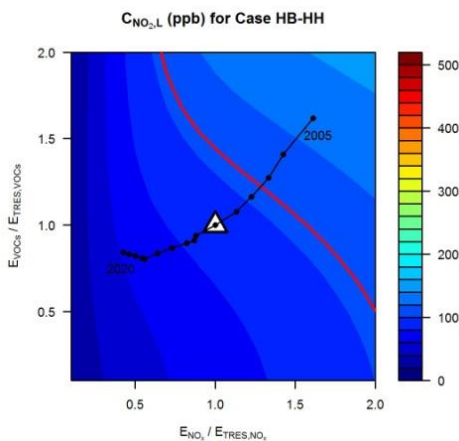
(d)



779

780

(e)



781

782

783

784

785

786

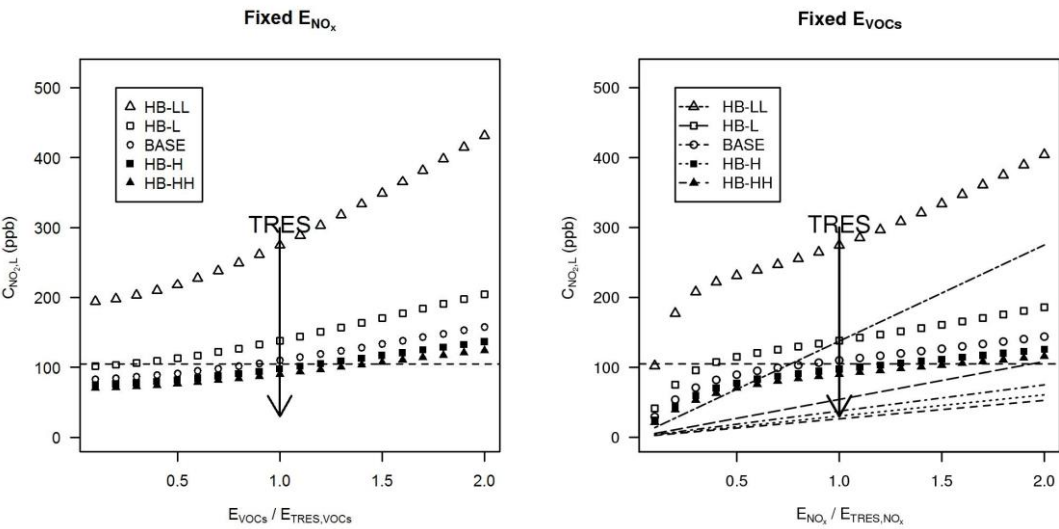
787

**Figure 12**  $C_{NO_2,L}$  (ppb), i.e. the concentration in the lower box derived from the “two-box” model, in the (a) Case HB-LL ( $\alpha = 0.1$ ), (b) Case HB-L ( $\alpha = 0.3$ ), (c) Case BASE ( $\alpha = 0.5$ ), (d) Case HB-H ( $\alpha = 0.7$ ), and (e) Case HB-HH ( $\alpha = 0.9$ ).  $E_{VOCs}$  and  $E_{NOx}$  are normalised by those of the Typical Real-world Emission Scenario (TRES, represented by  $\Delta$ ), for the year of 2010. Trajectory 2005-2020 represents the emission scenarios for 2005 to 2020, assuming constant traffic volume and speed. The solid red curves denote the UK air quality standard for hourly  $NO_2$  (105 ppb).

788

789

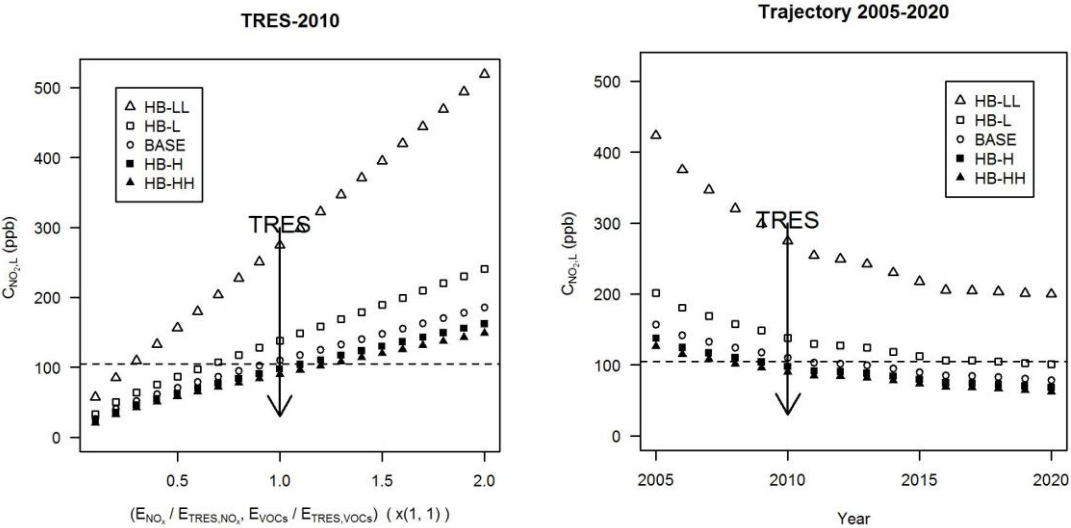
(a) (b)



790

791

(c) (d)



792

793

794

795

796

797

798

799

**Figure 13**  $C_{NO_2,L}$  (ppb), i.e. the concentration in the lower box derived from the “two-box” model, for (a) “Fixed  $E_{NO_x}$ ” at a fixed  $NO_x$  emissions of TRES, (b) “Fixed  $E_{VOCs}$ ” at a fixed  $VOCs$  emissions of TRES (The direct contributions of  $NO_x$  emissions to  $C_{NO_2,L}$  are indicated by a series of radiating lines, running from highest to lowest for the cases from HB-LL to HB-HH.), (c) “TRES-2010” varying the total traffic volume only and (d) “Trajectory 2005-2020” assuming constant traffic volume and speed varying  $\alpha \cdot E_{VOCs}$  and  $E_{NO_x}$  are normalised by those of the Typical Real-world Emission Scenario (TRES, represented by  $\Delta$ ), for the year of 2010. The dashed line indicates the UK air quality standard for hourly  $NO_2$  (105 ppb).

800

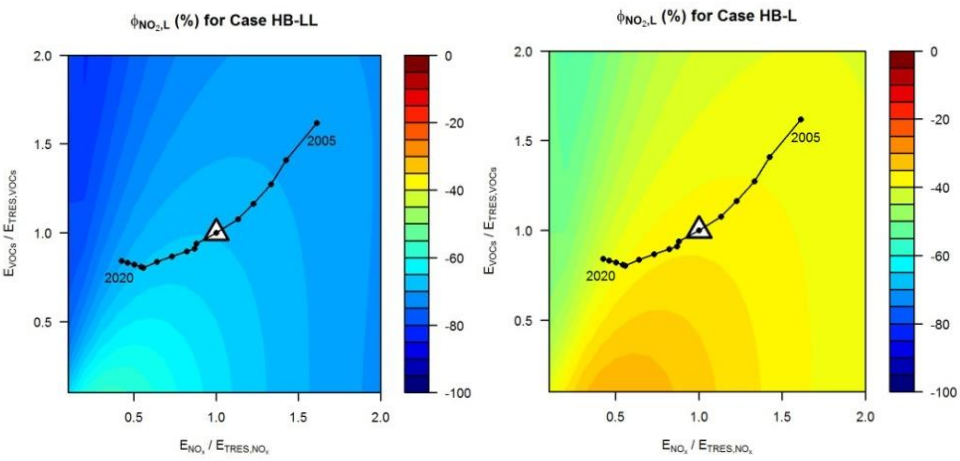
801

802

803

(a)

(b)

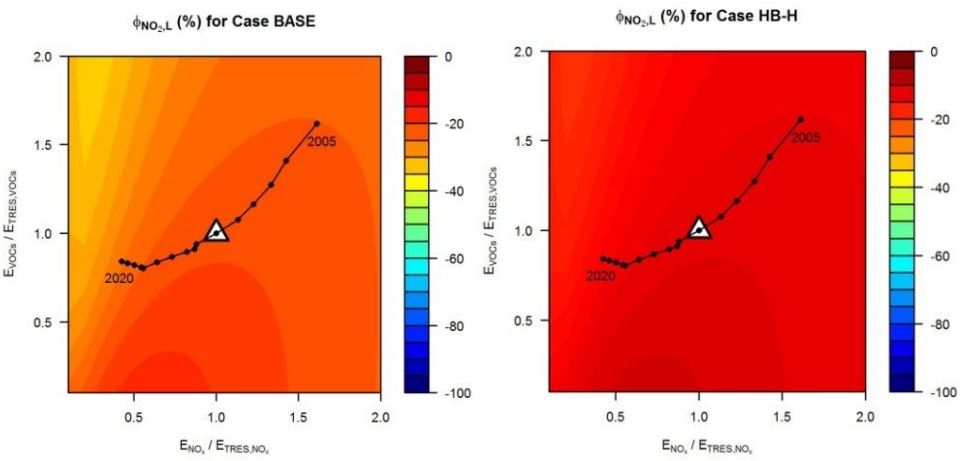


804

805

(c)

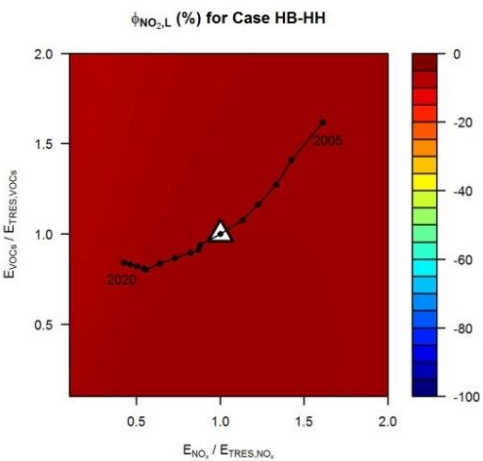
(d)



806

807

(e)



808

809

810

811

812

813

814

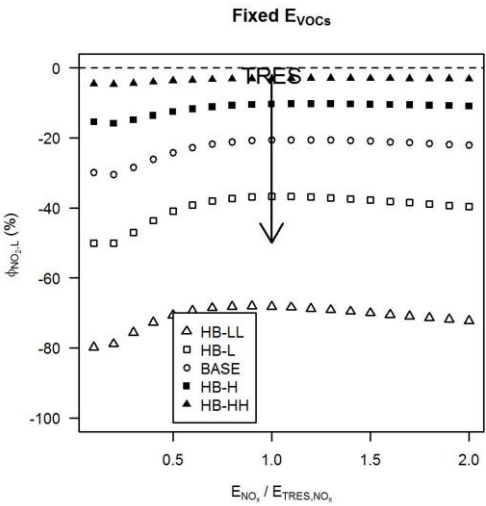
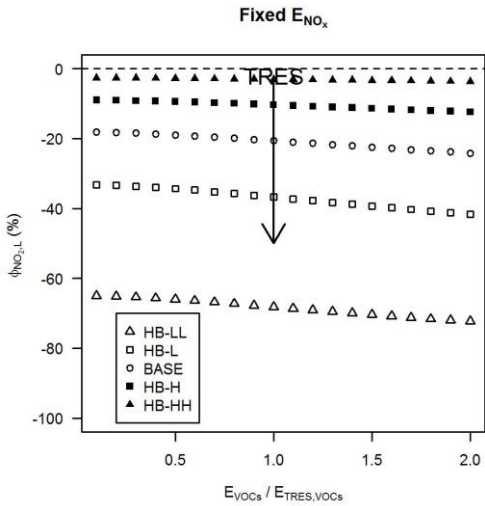
**Figure 14**  $\phi_{NO_2,L} (%)$ , i.e. the percentage of overestimation for  $NO_2$  in the lower canyon by the ‘one-box’ model compared with that by the “two-box” model, in the (a) Case HB-LL ( $\alpha=0.1$ ), (b) Case HB-L ( $\alpha=0.3$ ), (c) Case BASE ( $\alpha=0.5$ ), (d) Case HB-H ( $\alpha=0.7$ ), and (e) Case HB-HH ( $\alpha=0.9$ ).  $E_{VOCs}$  and  $E_{NOx}$  are normalised by those of the Typical Real-world Emission Scenario (TRES, represented by  $\triangle$ ), for the year of 2010. Trajectory 2005-2020 represents the emission scenarios for 2005 to 2020, assuming constant traffic volume and speed. The solid red curves denote the UK air quality standard for hourly  $NO_2$  (105 ppb).



815

(a)

(b)

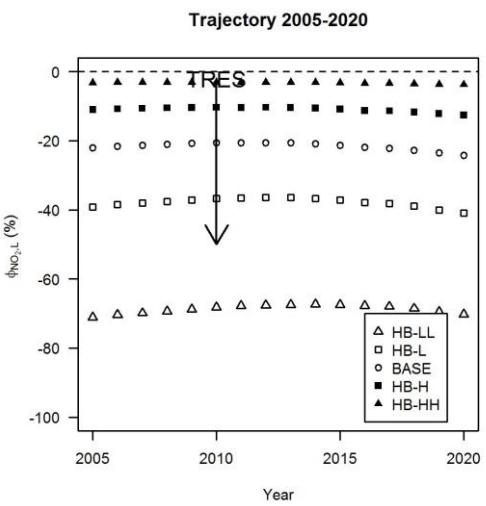
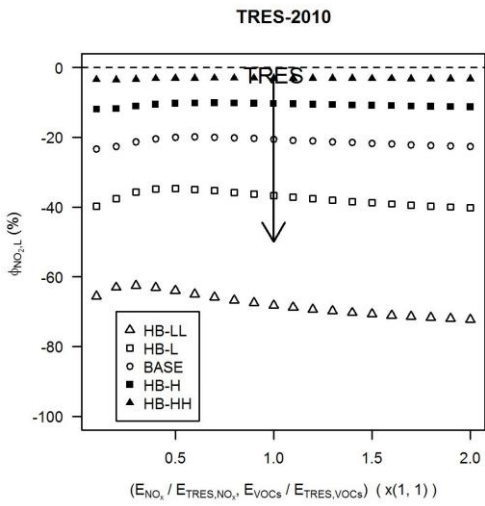


816

817

(c)

(d)



818

819

820

821

822

823

824

825

826

827

828

**Figure 15**  $\phi_{NO_2,L}$  (%), i.e. the percentage of overestimation for  $NO_2$  in the lower canyon by the ‘one-box’ model compared with that by the “two-box” model, for (a) “Fixed  $E_{NOx}$ ” at a fixed  $NO_x$  emissions of TRES, (b) “Fixed  $E_{VOCs}$ ” at a fixed VOCs emissions of TRES, (c) “TRES-2010” varying the total traffic volume only and (d) “Trajectory 2005-2020” assuming constant traffic volume and speed varying  $\alpha$ .  $E_{VOCs}$  and  $E_{NOx}$  are normalised by those of the Typical Real-world Emission Scenario (TRES, represented by  $\Delta$ ), for the year of 2010.

829 **References:**

- 830 BAKER, J., WALKER, H. L. & CAI, X. M. 2004. A study of the dispersion and transport of  
831 reactive pollutants in and above street canyons - a large eddy simulation. *Atmospheric*  
832 *Environment*, 38, 6883-6892.
- 833 BARLOW, J. F., HARMAN, I. N. & BELCHER, S. E. 2004. Scalar fluxes from urban street  
834 canyons. Part I: Laboratory simulation. *Boundary-Layer Meteorology*, 113, 369-385.
- 835 BOULTER, P. G., BARLOW, T. J., LATHAM, S. & MCCRAE, I. S. 2009. Emission Factors 2009:  
836 Report 1 - a review of methods for determining hot exhaust emission factors for road  
837 vehicles. *TRL: Wokingham*.
- 838 BRIGHT, V. B. 2013. *Street canyon atmospheric composition: coupling dynamics and chemistry*.  
839 Ph.D. thesis, University of Birmingham.
- 840 BRIGHT, V. B., BLOSS, W. J. & CAI, X. M. 2013. Urban street canyons: Coupling dynamics,  
841 chemistry and within-canyon chemical processing of emissions. *Atmospheric Environment*,  
842 68, 127-142.
- 843 BUCKLAND, A. T. 1998. Validation of a street canyon model in two cities. *Environmental*  
844 *Monitoring and Assessment*, 52, 255-267.
- 845 CARSLAW, D. & RHYS-TYLER, G. 2013. Remote sensing of NO<sub>2</sub> exhaust emissions from road  
846 vehicles. *A report to the City of London Corporation and London Borough of Ealing*.
- 847 CATON, F., BRITTER, R. E. & DALZIEL, S. 2003. Dispersion mechanisms in a street canyon.  
848 *Atmospheric Environment*, 37, 693-702.
- 849 DEFRA 2008. The Air Quality Strategy for England, Scotland, Wales and Northern Ireland.  
850 Volume 1.
- 851 GROMKE, C. & RUCK, B. 2012. Pollutant Concentrations in Street Canyons of Different Aspect  
852 Ratio with Avenues of Trees for Various Wind Directions. *Boundary-Layer Meteorology*,  
853 144, 41-64.
- 854 KWAK, K. H., BAIK, J. J. & LEE, K. Y. 2013. Dispersion and photochemical evolution of reactive  
855 pollutants in street canyons. *Atmospheric Environment*, 70, 98-107.
- 856 LI, X.-X., LIU, C.-H. & LEUNG, D. Y. C. 2008. Large-eddy simulation of flow and pollutant  
857 dispersion in high-aspect-ratio urban street canyons with wall model. *Boundary-Layer*  
858 *Meteorology*, 129, 249-268.
- 859 LI, X. X., BRITTER, R. E., NORFORD, L. K., KOH, T. Y. & ENTEKHABI, D. 2012. Flow and  
860 Pollutant Transport in Urban Street Canyons of Different Aspect Ratios with Ground  
861 Heating: Large-Eddy Simulation. *Boundary-Layer Meteorology*, 142, 289-304.
- 862 LI, X. X., LIU, C. H. & LEUNG, D. Y. C. 2009. Numerical investigation of pollutant transport  
863 characteristics inside deep urban street canyons. *Atmospheric Environment*, 43, 2410-2418.
- 864 LIU, C.-H., CHENG, W. C., LEUNG, T. C. Y. & LEUNG, D. Y. C. 2011. On the mechanism of air  
865 pollutant re-entrainment in two-dimensional idealized street canyons. *Atmospheric*  
866 *Environment*, 45, 4763-4769.
- 867 LIU, C.-H. & LEUNG, D. Y. C. 2008. Numerical study on the ozone formation inside street  
868 canyons using a chemistry box model. *Journal of Environmental Sciences-China*, 20, 832-  
869 837.
- 870 LIU, C. H., LEUNG, D. Y. C. & BARTH, M. C. 2005. On the prediction of air and pollutant  
871 exchange rates in street canyons of different aspect ratios using large-eddy simulation.  
872 *Atmospheric Environment*, 39, 1567-1574.
- 873 LOUKA, P., BELCHER, S. E. & HARRISON, R. G. 2000. Coupling between air flow in streets  
874 and the well-developed boundary layer aloft. *Atmospheric Environment*, 34, 2613-2621.
- 875 MURENA, F. 2012. Monitoring and modelling carbon monoxide concentrations in a deep street  
876 canyon: application of a two-box model. *Atmospheric Pollution Research*, 3, 311-316.
- 877 MURENA, F., DI BENEDETTO, A., D'ONOFRIO, M. & VITIELLO, G. 2011. Mass Transfer  
878 Velocity and Momentum Vertical Exchange in Simulated Deep Street Canyons. *Boundary-*  
879 *Layer Meteorology*, 140, 125-142.



880 MURENA, F. & FAVALE, G. 2007. Continuous monitoring of carbon monoxide in a deep street  
881 canyon. *Atmospheric Environment*, 41, 2620-2629.

882 MURENA, F., FAVALE, G., VARDOULAKIS, S. & SOLAZZO, E. 2009. Modelling dispersion of  
883 traffic pollution in a deep street canyon: Application of CFD and operational models.  
884 *Atmospheric Environment*, 43, 2303-2311.

885 MURENA, F., GAROFALO, N. & FAVALE, G. 2008. Monitoring CO concentration at leeward  
886 and windward sides in a deep street canyon. *Atmospheric Environment*, 42, 8204-8210.

887 NAEI 2003. UK fleet composition projections. URL: <http://naei.defra.gov.uk/data/ef-transport>.

888 OKE, T. R. 1987. Boundary Layer Climates. *second ed*, Methuen, London.

889 PUGH, T. A. M., MACKENZIE, A. R., WHYATT, J. D. & HEWITT, C. N. 2012. Effectiveness of  
890 Green Infrastructure for Improvement of Air Quality in Urban Street Canyons.  
891 *Environmental Science & Technology*, 46, 7692-7699.

892 RAMAMURTHY, P., PARDYJAK, E. R. & KLEWICKI, J. C. 2007. Observations of the effects of  
893 atmospheric stability on turbulence statistics deep within an urban street canyon. *Journal of*  
894 *Applied Meteorology and Climatology*, 46, 2074-2085.

895 SAHM, P., LOUKA, P., KETZEL, M., GUILLOTEAU, E. & SINI, J. F. 2002. *Intercomparison of*  
896 *numerical urban dispersion models - Part I: Street canyon and single building*  
897 *configurations*.

898 SALIM, S. M., BUCCOLIERI, R., CHAN, A. & DI SABATINO, S. 2011. Numerical simulation of  
899 atmospheric pollutant dispersion in an urban street canyon: Comparison between RANS and  
900 LES. *Journal of Wind Engineering and Industrial Aerodynamics*, 99, 103-113.

901 SALIZZONI, P., SOULHAC, L. & MEJEAN, P. 2009. Street canyon ventilation and atmospheric  
902 turbulence. *Atmospheric Environment*, 43, 5056-5067.

903 ZHONG, J., CAI, X. & BLOSS, W. J. 2014. Modelling segregation effects of heterogeneous  
904 emissions on ozone levels in idealised urban street canyons: Using photochemical box  
905 models *Environmental Pollution*, 188, 132-143.

906 ZHONG, J., CAI, X. & BLOSS, W. J. 2015. Modelling the dispersion and transport of reactive  
907 pollutants in a deep urban street canyon: Using large-eddy simulation. *Environmental*  
908 *Pollution*, 200, 42-52.

909 ZHONG, J., CAI, X. & BLOSS, W. J. 2016. Coupling dynamics and chemistry in the air pollution  
910 modelling of street canyons: A review. *Environmental Pollution*, 214, 690-704.

911

912